WATER RESOURCES RESEARCH, VOL. 49, 5183–5205, doi:10.1002/wrcr.20391, 2013

Hydraulic validation of two-dimensional simulations of braided river flow with spatially continuous aDcp data

R. D. Williams,[1] J. Brasington,[2] M. Hicks,[3] R. Measures,[3] C. D. Rennie,[4] and D. Vericat[1,5,6]

Received 21 February 2013; revised 20 June 2013; accepted 22 June 2013; published 4 September 2013.

[1] Gravel-bed braided rivers are characterized by shallow, branching flow across low relief, complex, and mobile bed topography. These conditions present a major challenge for the application of higher dimensional hydraulic models, the predictions of which are nevertheless vital to inform flood risk and ecosystem management. This paper demonstrates how high-resolution topographic survey and hydraulic monitoring at a density commensurate with model discretization can be used to advance hydrodynamic simulations in braided rivers. Specifically, we detail applications of the shallow water model, Delft3d, to the Rees River, New Zealand, at two nested scales: a 300 m braid bar unit and a 2.5 km reach. In each case, terrestrial laser scanning was used to parameterize the topographic boundary condition at hitherto unprecedented resolution and accuracy. Dense observations of depth and velocity acquired from a mobile acoustic Doppler current profiler (aDcp), along with low-altitude aerial photography, were then used to create a data-rich framework for model calibration and testing at a range of discharges. Calibration focused on the estimation of spatially uniform roughness and horizontal eddy viscosity, ν_H, through comparison of predictions with distributed hydraulic data. Results revealed strong sensitivity to ν_H, which influenced cross-channel velocity and localization of high shear zones. The high-resolution bed topography partially accounts for form resistance, and the recovered roughness was found to scale by 1.2–1.4 D_{84} grain diameter. Model performance was good for a range of flows, with minimal bias and tight error distributions, suggesting that acceptable predictions can be achieved with spatially uniform roughness and ν_H.

Citation: Williams, R. D., J. Brasington, M. Hicks, R. Measures, C. D. Rennie, and D. Vericat (2013), Hydraulic validation of two-dimensional simulations of braided river flow with spatially continuous aDcp data, *Water Resour. Res.*, *49*, 5183–5205, doi:10.1002/wrcr.20391.

1. Introduction

1.1. Numerical Modeling

[2] Two-dimensional (2-D) numerical models are widely used to simulate flow depth and depth-averaged velocity in rivers to investigate instream habitat [e.g., *Pasternack et al*., 2004; *Stewart et al*., 2005; *Papanicolaou et al*., 2011b; *Jowett and Duncan*, 2012], assess the impact of hydro-operations [e.g., *Hicks et al*., 2009], map critical hydraulic conditions [*Hodge et al*., 2013], and simulate morphological change [e.g., *Murray and Paola*, 1997; *Coulthard et al*., 2002; *Nicholas and Quine*, 2007; *Rinaldi et al*., 2008]. Over the last decade, the proliferation of new streams of remotely sensed data has sustained continuous progress in the construction, parameterization, calibration, and validation of high-resolution 2-D hydraulic models [*Bates*, 2012; *Di Baldassarre and Uhlenbrook*, 2012]. In addition, computational developments including parallelization [e.g., *Rao*, 2005; *Neal et al*., 2010] and graphics processing unit hardware [e.g., *Lamb et al*., 2009; *Kalyanapu et al*., 2011] have facilitated the considerable gains in model run times. Despite these developments, comparatively little attention has focused on evaluating the performance of models to simulate flow across morphologically complex river beds, such as braided rivers. For the case of morphological simulations, the accuracy of 2-D hydraulic predictions is paramount as they combine nonlinearly in sediment transport algorithms to calculate morphological evolution.

[3] There has been considerable interest in exploiting the computational efficiency of reduced complexity [*Murray*, 2007] frameworks to simulate morphological evolution over decadal to centurial timescales [e.g., *Coulthard et al*., 2002; *Thomas et al*., 2007; *Van De Wiel et al*., 2007]. The morphologies simulated by reduced complexity

[1]Department of Geography and Earth Sciences, Aberystwyth University, Aberystwyth, UK.
[2]School of Geography, Queen Mary, University of London, London, UK.
[3]National Institute of Water and Atmospheric Research, Christchurch, New Zealand.
[4]Department of Civil Engineering, University of Ottawa, Ottawa, Ontario, Canada.
[5]Fluvial Dynamics Research Group (RIUS), Department of Environment and Soil Sciences, University of Lleida, Lleida, Spain.
[6]Hydrology Section, Forest Sciences Center of Catalonia, Solsona, Catalunya, Spain.

Corresponding author: R. D. Williams, Institute of Geography and Earth Sciences, Aberystwyth University, Penglais Campus, Aberystwyth, Ceredigion SY23 3DB, UK. (rdw5@aber.ac.uk)

©2013. American Geophysical Union. All Rights Reserved.
0043-1397/13/10.1002/wrcr.20391

frameworks can, however, be unrealistic [*Doeschl-Wilson and Ashmore*, 2005], suggesting that the governing equations are overly simplified and a stronger physical basis may be necessary to generate behavioral model outcomes. Integrating shallow water equations into morphological simulation models may enhance their performance and, when performing unsteady simulations, may not lead to significant losses in terms of computational efficiency [*Nicholas et al*., 2012]. There is thus a pressing need to acquire precise and high-resolution observational data, in a morphologically complex setting such as a braided river, to validate the predictions of hydraulic modeling frameworks based on 2-D shallow water equations.

1.2. Model Topography

[4] Accurate topographic data are a primary control on the quality of two-dimensional model predictions [*Bates and De Roo*, 2000]. The sensitivity of simulation results to topographic uncertainty has been examined recently by *Legleiter et al*. [2011] using a two-dimensional model of a single-thread, meandering channel. These authors found that predictive uncertainty was greater when survey data were degraded, that model sensitivity was inversely related to discharge, and predictions were particularly sensitive to elements of topography that steer flow, such as point bars. Accurate topographic modeling of braided rivers has received significant interest, prompted by the difficulties of simultaneously surveying the exposed braidplain relief and wetted channel elevations in comparatively shallow anabranches [*Hicks*, 2012]. Ground-based approaches, such as real-time kinematic (RTK) GPS, have been shown to be effective in this situation [*Brasington et al*., 2000] but are restricted to relatively small reaches due to logistical constraints. The acquisition of continuous topographic data by remote survey methods, more suitable for modeling large rivers, by contrast, typically requires the fusion data from more than one survey method. For example, digital elevation models (DEMs) have been built using photogrammetry and digital tacheometry [*Lane et al*., 1994] or by fusing together optical-empirical bathymetric maps with airborne LiDAR [*Hicks et al*., 2001; *Brasington et al*., 2003; *Lane et al*., 2003], airborne photogrammetry [*Westaway et al*., 2003], or terrestrial laser scanning [TLS, *Williams et al*., 2011, 2013]. A recent study by Milan and Heritage [*Milan and Heritage*, 2012] also demonstrates the potential for coupling TLS with bathymetric surveys acquired using moving boat deployment of acoustic Doppler current profilers (aDcp). Since the fusion of TLS with aDcp does not require an intermediate processing step to map water surface elevations, channel bed levels are mapped to decimeter accuracy. This accuracy is similar to that obtained from bathymetric mapping using either empirical-optical modeling [*Marcus and Fonstad*, 2008; *Marcus*, 2012] or green-blue LiDAR [*Hilldale and Raff*, 2008; *McKean et al*., 2008; *Bailly et al*., 2010].

[5] Terrestrial laser scanning, in particular, offers the potential to survey accurately small-scale features in braidplain morphology due to the high point precision (2–4 mm in xyz) and dense-point spacing (sub-cm) associated with the technique [*Milan et al*., 2007; *Brasington et al*., 2012; *Williams et al*., 2013]. Although TLS has not yet been combined with hydraulic modeling in a natural floodplain environment, *Sampson et al*. [2012] and *Fewtrell et al*. [2011] demonstrate the value of using TLS-derived DEMs to simulate the routing of shallow flood water in urban environments where small-scale topographic features, such as street curbs and road surface camber, can influence the routing of floodwater. Significantly, *Sampson et al*. [2012] show that the small-scale features that are represented in TLS-derived DEMs, but not evident in airborne LiDAR-derived DEMs, are preserved when DEMs are degraded from 10 cm to 1 m horizontal resolution. TLS-derived DEMs are thus capable of maintaining hydraulic connectivity through small-scale topographic undulations that would not be represented in DEMs derived using alternative geomatics technologies that are characterized by lower precision and sparser point density.

1.3. Depth and Velocity Observations

[6] Acquiring distributed depth and velocity observations to validate the predictions of numerical models in the morphologically and hydraulically complex setting of multithread channels is logistically challenging. Moving boat deployment of aDcps, coupled with RTK-GPS for accurate three-dimensional positioning, offers considerable potential for collecting both hydraulic and bathymetric data [*Muste et al*., 2012]. In medium to large single-thread rivers, aDcps have been deployed on propelled boats that are navigated along closely spaced transects to survey flow features [e.g., *Muste et al*., 2004; *Rennie and Millar*, 2004; *Dinehart and Burau*, 2005; *Parsons et al*., 2006; *Rennie and Church*, 2010; *Guerrero and Lamberti*, 2011; *Jamieson et al*., 2011]. In large multithread rivers, boat-mounted aDcps have been used to investigate flow features in both diffluence [*Richardson and Thorne*, 2001] and confluence units [*Szupiany et al*., 2009]. In narrower riverine settings, *Riley and Rhoads* [2012] mapped flow characteristics and bed elevations along 13 transects across a natural confluent meander bend using an aDcp mounted on a polyethylene trimaran and zigzagged across channels using tethers. *Entwistle et al*. [2010] also demonstrate the potential for using a tethered boat to map depth-averaged flow features along a 40 m wide and 150 m long channel that bifurcates around a gravel bar at low flow. There are, however, no examples of moving boat surveys at multiple flow stages in braided gravel-bed rivers.

[7] Acoustic instrumentation has been widely used to validate numerical flow models. *Lane et al*. [1999], for example, use acoustic Doppler velocimeter (aDv) measurements distributed throughout a confluence unit to assess flow structure predictions of 2-D and 3-D models. A similarly distributed approach is utilized by *Pasternack et al*. [2006], who measured depth and velocity profiles at 23 locations, although they also validated their 2-D model using measurements along two transects. Such a transect-based approach is common in reach-scale modeling of single thread rivers [e.g., *Barton et al*., 2005; *Milan*, 2009; *Ruther et al*., 2010; *Papanicolaou et al*., 2011b; *Guerrero et al*., 2013] and braided rivers [e.g., *Thomas and Nicholas*, 2002; *Jowett and Duncan*, 2012; *Nicholas et al*., 2012]. However, assessing the predictions of numerical models based upon flow observations at transects that are longitudinally spaced at distances of more than one anabranch width can produce observational data that do not incorporate

spatially varying flow features, particularly those at diffluences and confluences where flow character changes relatively rapidly in the streamwise direction. Spatially intensive sampling of flow velocities has been reported by *Clifford et al*. [2005, 2010] who collected 300 data points at transverse and longitudinal intervals of approximately 0.5 m and 1–2 m, respectively, to assess the predictions of a 3-D model. Such observations enabled these authors to consider the spatial semivariance between modeled and measured velocities, indicating that major flow features were well predicted. Overall, however, most simulation predictions have been compared using flow observations obtained along multiple transverse transects rather than exploiting the potential of moving boat aDcp deployments to provide spatially distributed observations for model validation. Although *Milan and Heritage* [2012] demonstrate the potential for generating topography from a fusion of TLS and aDcp surveys to simulate a range of flows using a 2-D numerical model, their velocity results are used to map changes in biotope extents rather than validating model performance. The potential for utilizing spatially dense aDcp data to both map bathymetry and assess model hydraulic predictions is yet to be utilized in braided river environments.

[8] Whilst acquiring spatially continuous aDcp surveys of water velocity and depth during high flows is feasible using boat deployments in big rivers, for shallow gravel-bed rivers such measurements are inhibited by access problems. Validating model performance of relatively shallow rivers is therefore most commonly approached using maps of observed inundation extent. Simple measures are widely used to compare predicted flood extents to remotely sensed observations from both airborne and satellite platforms [*Bates and De Roo*, 2000; *Horritt*, 2000]. Considerable progress has been made in urban flood inundation modeling using simple areal extent measures, particularly when validating ensembles of simulations [*Aronica et al*., 2002; *Bates et al*., 2004; *Horritt*, 2006]. In rural settings, areal extent measures are ineffective in topographically constricted valley settings but in braided reaches the complex nature of topography provides a relatively rigorous test for comparing model predictions to observations. The potential for obtaining photographs of braided river inundation extents at a range of flows has been shown by *Ashmore and Sauks* [2006], using orthorectified oblique images.

1.4. Objectives and Structure

[9] The first objective of this paper is to demonstrate the capability of 2-D shallow water wave models for accurately predicting both water level and depth-averaged velocity in shallow braided rivers. A second objective is to investigate whether calibration of spatially constant roughness and horizontal eddy viscosity values can deliver robust predictions. The final objective is to investigate the effects of grid resolution, horizontal eddy viscosity, roughness, and model wetting and drying threshold on model performance. Figure 1 summarizes the mesoscale and macroscale modeling approaches that are used to calibrate and validate [*Refsgaard and Henriksen*, 2004] the 2-D model. Throughout this paper, the terminology of *Refsgaard and Henriksen* [2004] is used to define calibration and validation. At the mesoscale, spatially dense aDcp observations are used to parameterize the model. This parameterization is then transferred to the macroscale, where model performance is assessed using aerial images of inundation extent and aDcp observations from streamwise surveys.

[10] The following sections describe the study site, outline the methods that were used to survey braidplain topography, and acquire high-resolution information on flow dynamics, and describe the experimental framework (Figure 1). The next section presents results from the sets of simulations undertaken at mesoscale and macroscales, with an emphasis on the most appropriate parameterizations. A discussion follows that examines the hydraulic predictions, parameter and scale compensation effects, assesses the potential value of further uncertainty analysis, and finally considers the implications for morphodynamic simulations.

2. Study Site

2.1. Rees River Catchment and Hydrology

[11] This paper focuses upon validating the performance of hydraulic models developed to simulate the flow of the braided, gravel-bed, Rees River. The 420 km^2 Rees catchment is located in the South Island, New Zealand, to the east of the Southern Alps (Figure 2a). The morphodynamics of a 2.5 km long reach of the Rees River have recently been monitored as part of the ReesScan Project [*Brasington*, 2010]. The Rees was chosen for this monitoring campaign because it is very morphologically active and has manageable spatial dimensions and hydraulic energy levels for data acquisition. The Rees' upper catchment is dominated by relatively erodible schist, belonging to the Mount Aspiring lithologic association [*Turnbull*, 2000]. Through its upper reaches, the Rees is typically confined to a single channel, with high mountain peaks rising above the valley floor to altitudes in excess of 2000 m and glaciers sitting upon the high, south-facing slopes of the Forbes Mountains. The combination of tectonic uplift, a relatively weak bedrock, thin soil and vegetation cover, and frequent storm events causes regular landslides and large alluvial fans extend from tributaries. The Rees flows through a bedrock gorge before emerging at the mountain front where the valley floor is dominated by Holocene alluvial deposits derived from the upper catchment's easily erodible schist. The Rees has developed a wide, labile, braided gravel-bed [*Otago Regional Council*, 2008; *Williams et al*., 2011] that extends downstream to an extensive delta that is prograding into Lake Wakatipu [*Wild et al*., 2008]. Historic aerial photographs, acquired infrequently between 1937 and 2006, show that the reach downstream of the mountain front is very dynamic, with frequent avulsions. Repeat cross-section surveys undertaken between 1984 and 2006 suggest that the braidplain is slowly aggrading [*Otago Regional Council*, 2008].

[12] Precipitation in the region is characterized by strong orographic gradients due to the high elevations of the Southern Alps and their proximity to the Tasman Sea. Mean annual precipitation (1988–2011) at Rees Valley Station, situated in the lower catchment, is 1462 mm. The Rees River's flow is dominated by storm events that generate steep rising limbs (Figure 3) due to the catchment's steep slopes and thin soil cover. Flow was recorded at the Invincible gauging station (Figure 2b) from September

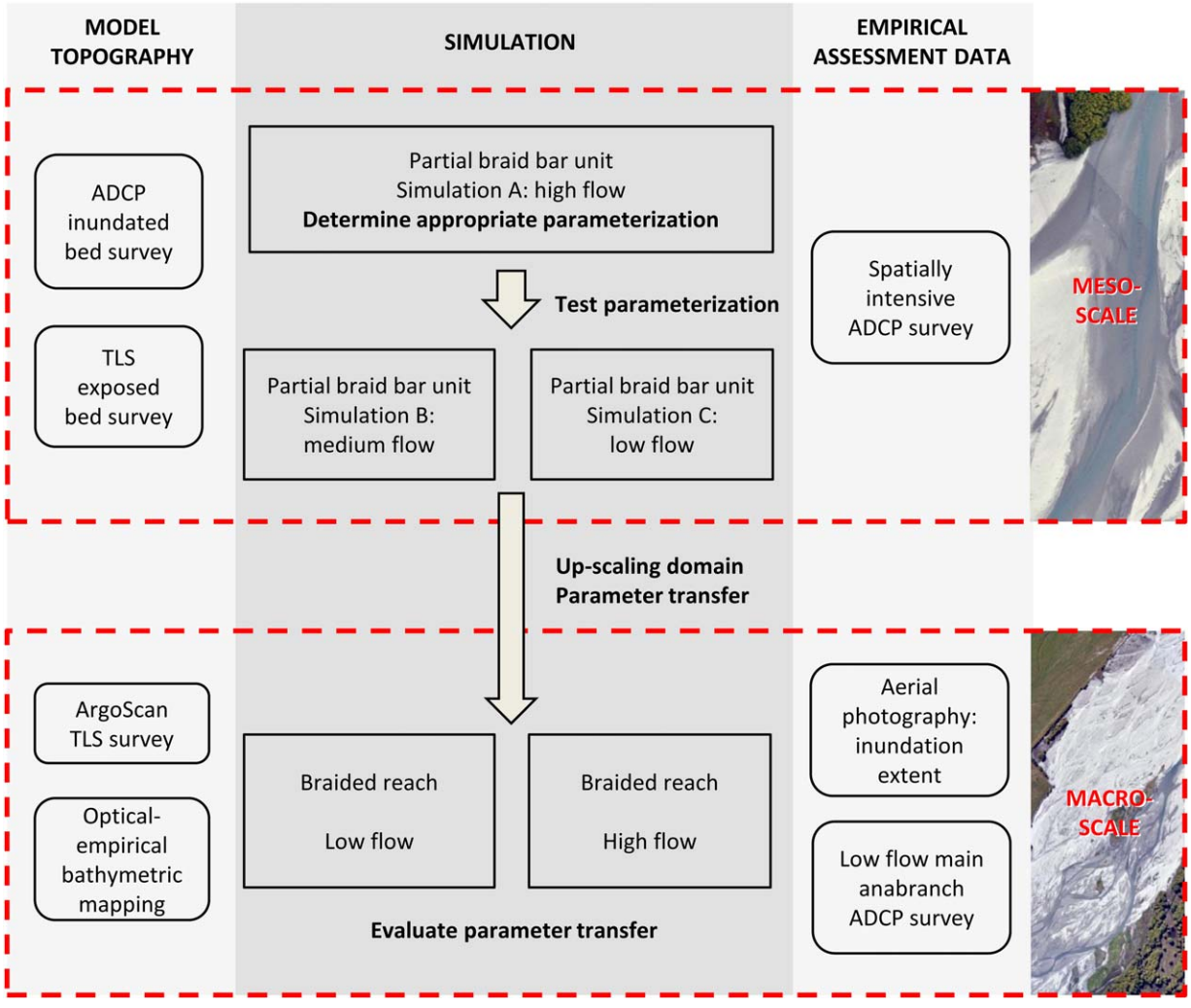

Figure 1. Experimental framework.

2009 to March 2011. For the 2010–2011 hydrological year, starting in April, mean discharge was 20.0 $m^3 s^{-1}$. During the entire gauging period, the highest three flows were 407, 419, and 475 $m^3 s^{-1}$. Whilst a long-term flow record is not available for the Rees, comparison with a 13 year long flow record from the adjacent Dart catchment indicate that these high-flow events all exceeded the mean annual maximum flow.

2.2. Braided Reach

[13] Data collection concentrated on a braided reach located approximately equidistant from the mountain front and the delta at Lake Wakatipu (Figure 2b). Topographic and hydraulic survey data were acquired at the braided reach (macroscale) as part of the ReesScan Project [*Brasington*, 2010; *Williams et al*., 2011, 2013], which featured an eight-month long field campaign to monitor the evolution of a 2.5 by 0.8 km braided reach (Figure 2c) through a sequence of storm events from September 2009 to May 2010. This paper focuses upon survey data that were collected over the braided reach (macroscale) during the falling limb of the storm event that occurred on 22 March 2010 and peaked at 320 $m^3 s^{-1}$ (Figure 3a). A subsequent field campaign, in early 2011, monitored the evolution of a partial braid bar unit (mesoscale; Figure 2d) during the falling limb of a storm event on 6 February 2011. This storm event peaked at 475 $m^3 s^{-1}$ (Figure 3b). This was the highest flow recorded during the September 2009 to March 2011 gauging period.

[14] Lateral migration of the 2.5 km long braided reach (Figure 2c) is primarily constrained by Crack willow (*Salix fragilis*) plantations on the left bank and a network of earth and rock armor stop-banks on the true right bank. The braided reach has a mean longitudinal gradient of approximately 1:200. During storms, braiding intensity first increases with discharge but then declines during large events that inundate almost the entire braidplain. At low flows, such as that shown in Figure 2c, 7% of the braidplain is typically inundated. The braidplain fairway (i.e., the active width) is primarily covered by unconsolidated gravels, although there are several vegetated islands where the dominant species is Russell lupin (*Lupinus polyphyllus*).

[15] Surface grain size distributions in the braided study reach were sampled to link the calibrated hydraulic model bed roughness to grain roughness. Surface material was sampled by means of the grid-count technique. This

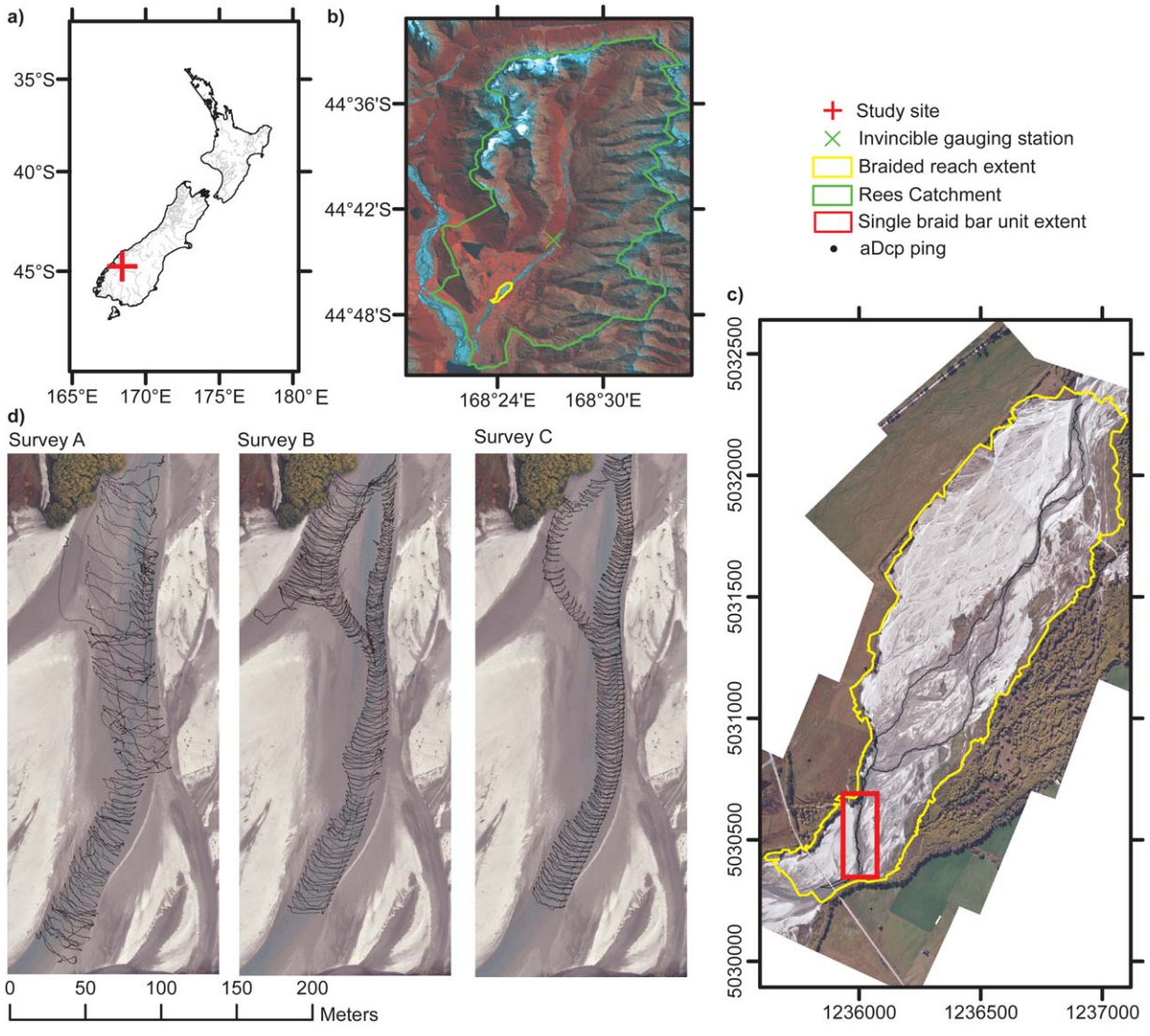

Figure 2. (a) Location of study area. (b) False color composite multispectral SPOT image of the Rees catchment. (c) Extent of braided reach and track of aDcp low-flow survey on 10 April 2010 (aerial photo also taken on this date), grid in New Zealand Transverse Mercator (NZTM), m. (d) aDcp transects for partial braid bar unit surveys A, B, and C (see Table 1 for survey times; aerial photo taken on 27 February 2011, after a storm event subsequent to survey C that caused morphological evolution of the braidplain).

technique is equivalent to the *Wolman* [1954] pebble count approach. The intermediate axes of 100 clasts even-space selected from a 1 m^2 sample frame were measured. A spatially focused sampling strategy [*Bunte and Abt*, 2001] was adopted, with the sampling frame randomly positioned at 28 sites. Surface grain size distributions (Figure 4), with associated standard deviations, are characterized by $D_{16} = 10.4 \pm 5.0$, $D_{50} = 19.9 \pm 10.4$, $D_{84} = 35.2 \pm 19.2$, and $D_{90} = 40.5 \pm 21.9$ mm, where 16, 50, 84, and 90 represent the percentiles of the surface grain distribution. Surface sediments are typically bladed, reflecting the strong foliation and relative ease of parting that is characteristic of schist lithology. In the context of braided rivers in New Zealand, the particle size of the study reach is toward the finer end of the scale.

[16] Figure 2c shows the location of a 300 m long single braid bar confluence-diffluence unit that was intensively monitored in early 2011. The results of the topographic, apparent bedload transport, depth and velocity mapping undertaken during this campaign are summarized in *Rennie et al*. [2012]. An aerial photo of the partial braid bar unit is shown in Figure 2d, with the aDcp transects surveyed at three different stages overlaid. The aerial image was acquired following a storm event that caused some minor morphological evolution, although the overall structure of the braided network was maintained through the event.

3. Data Collection

3.1. Partial Braid Bar Unit (Mesoscale)

3.1.1. Depth and Velocity Data: Observations and Processing

[17] Spatially distributed surveys of depth and velocity were acquired across the partial braid bar unit using a

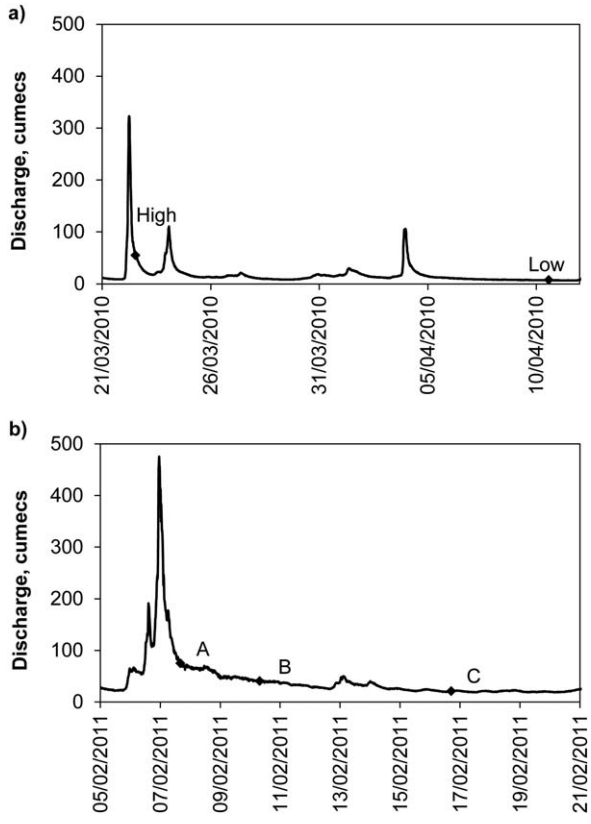

Figure 3. Hydrographs at Invincible Gauge for the high-flow events used for numerical simulations. (a) Braided reach (macroscale) showing time of high-flow and low-flow aerial photographs. (b) Partial braid bar unit (mesoscale) showing time of surveys A, B, and C.

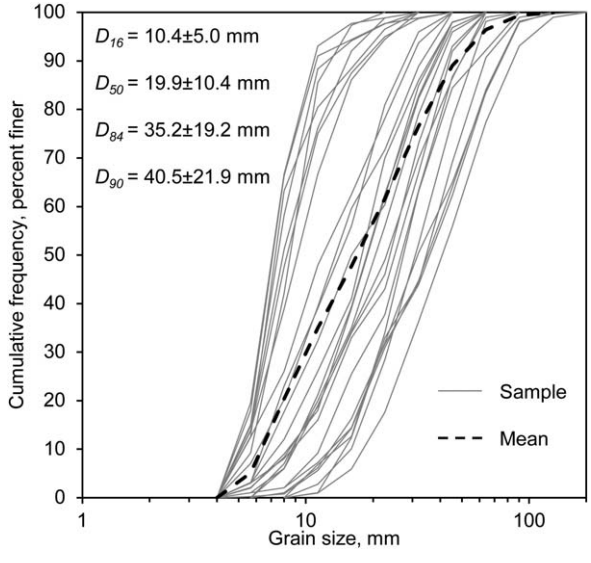

Figure 4. Surface grain size distributions for the braided reach (macroscale); 100 clast samples were measured at 28 sites using the grid count technique. This technique is equivalent to the pebble count approach first developed by *Wolman* [1954].

Sontek M9 RiverSurveyor aDcp (see *Simpson and Oltman* [1993], *Morlock* [1995], and *Muste et al*. [2004] for aDcp theory). The M9 RiverSurveyor used four 3 MHz transducers, rather than four 1 MHz transducers, due to shallow flow conditions. Three data sets were acquired, at a range of discharges, on the falling limb of a high-flow event that peaked at 475 m^3 s^{-1} on the evening of 6 February 2011 (Figure 3 and Table 1). The aDcp was installed on an Oceanscience Riverboat ST trimaran. Before launch, compass calibration was undertaken at the upstream end of the survey reach by rotating the aDcp and trimaran in two complete circles, with varying pitch and roll. Local magnetic interference was very low. The trimaran was tethered at the bow with ropes. These ropes were held by operators who stood on either side of an anabranch and maneuvered the boat downstream in closely spaced transects with a nominal spacing of 1–2 m (Figure 2d). The longitudinal spacing of transects was less uniform for the high-flow transects, compared to the surveys at low and medium flow, due to difficulties maintaining consistent zigzag trajectories at high velocities. Each survey was acquired in less than 4 h. Table 1 lists the discharges gauged at Invincible at the start and end of each survey. During survey A, discharge fell by 4.3 m^3 s^{-1} at Invincible. However, not all flow that was gauged at Invincible was routed through the mesoscale study area, and so the drop in discharge within the survey reach is likely to have been smaller in magnitude. For surveys B and C, discharges at Invincible increased by 0.3 and 1.0 m^3 s^{-1} during each survey, respectively. These variations are considered acceptable since they are comparable in magnitude to the variation in discharge that was gauged at the upstream end of the study reach at the start of each survey (Table 1). A Novatel RTK-GPS was mounted on the Riverboat to receive corrections from a GPS base station, thus providing centimeter-scale horizontal and vertical positional accuracy for each aDcp sample. Due to the immersion of the aDcp transducers and a blanking distance, the minimum depth that could be measured was 0.25 m; 1 Hz ensembles were derived from 10 Hz sampling. This yielded over 10,000 sample points per survey (Table 1), with a mean spacing of approximately 0.5 m along each transect. At each sample point, the data logger recorded georeferenced water surface elevation, water depth, bed elevation, and 0.1 m vertical bins of velocity in the x and y directions. Table 1 summarizes the depth and depth-averaged velocities measured during each survey.

[18] Mean depth was calculated at each sample location from the four bottom tracking depth estimates. Since each transducer is configured with a 25° slant angle, this results in the radius of the bed sampling area being approximately half the depth. Thus, compared to using data from the RiverSurveyor's 1.0 MHz vertical echo sounder, this approach enables some averaging of bed irregularities. Depth-averaged velocity magnitudes were calculated from the raw x and y velocity components for each measurement point. These processed point estimates of velocity and depth were used to assess the accuracy of simulated depths and velocities.

3.1.2. Topography

[19] Exposed braidplain topography was surveyed after each aDcp survey using a Leica 6100 phase-based terrestrial laser scanner with a range of 79 m at 90% albedo. For

Table 1. Descriptions of Timing, Sampling, Discharge, and Flow Characteristics of the Three Partial Braid Bar Unit (Mesoscale) Transect Surveys

Survey		A	B	C
Date		7 February 2011	10 February 2011	16 February 2011
Number of sample points/duration of survey, s		10,233	13,162	10,997
Surveyed depth[a], m	Mean	0.53	0.45	0.43
	Standard deviation	0.23	0.17	0.13
	Maximum	1.16	1.15	0.91
Surveyed depth-averaged velocity[a], ms^{-1}	Mean	1.63	1.36	1.41
	Standard deviation	0.47	0.40	0.34
	Maximum	2.68	2.74	2.34
Discharge at upstream boundary of survey[b], $m^3\ s^{-1}$		35.6 ± 0.9	23.6 ± 0.7	14.4 ± 0.7
Invincible gauge discharge[c], $m^3\ s^{-1}$	Start of survey	75.0	40.4	20.7
	End of survey	70.7	40.7	21.7
	Difference during survey	−4.3	+0.3	+1.0

[a]Statistics are based on all sample points, which were irregularly spaced.
[b]Discharge error refers to one standard deviation of the mean discharge measured from at least four aDcp transects.
[c]Not all flow was routed down the anabranches in the mesoscale unit.

each survey, 14–16 scans were acquired from stations distributed alongside each anabranch. The maximum distance between scan stations was 50 m. A control network was provided using two reflective targets that were positioned using RTK-GPS in static mode. Each target was located 10–15 m from the scanner. The mean three-dimensional point quality of the RTK-GPS positions was 9 mm (standard deviation was 2 mm). The TLS data were processed using the technique described in *Williams et al*. [2011]. In summary, individual point clouds were first georeferenced to the New Zealand Transverse Mercator (NZTM) Projection, using the RTK-GPS positions. All least-square cloud transformations yielded target standard deviations for the difference between point cloud and RTK-GPS target positions of less than 10 mm in each dimension. This error was deemed acceptable for the purpose of generating DEMs for hydraulic modeling. Each georeferenced point cloud was then unified into a single point cloud of 64–80 million survey points. The unified point cloud was then decimated to a quasi-uniform point spacing of 0.02 m and manually edited to remove objects and artifacts not associated with the braidplain's gravel-bed. The cleaned point cloud was then spatially filtered at a 0.25 m resolution using the ToPographic Point Cloud Analysis Toolkit (ToPCAT) [*Brasington et al*., 2012; *Rychkov et al*., 2012] to produce raster elevation grids based on the local minimum elevation.

[20] To produce a continuous topographic grid, for each survey, the TLS-derived minimum elevation exposed braidplain grid was fused with a grid of bed elevations derived from aDcp survey. For each aDcp data set of bed elevations, an anisotropic spherical model variogram was fitted to the observed variogram, using Surfer software and the same method described by *Rennie and Church* [2010]. The bed elevation observations were then gridded using ordinary kriging at a 0.5 m horizontal resolution. Figure 5a shows the DEM for Survey B. Kriging was chosen for interpolation because it smoothed measurement errors in irregularly spaced aDcp bed elevation survey points.

3.2. Braided Reach (Macroscale)

3.2.1. Topography

[21] The larger (macro) scale application focuses on a 2.5 km long reach of the Rees, surveyed in low-flow conditions following a storm event that peaked at 05:45 on 22 March 2010. The methodology used to produce the DEM is detailed by *Williams et al*. [2013]. In brief, the exposed topography was surveyed by acquiring TLS data at 318 scan stations using the ArgoScan system. These data were georeferenced, registered, cleaned, and filtered using ToPCAT to generate a bare-earth surface representation [*Brasington et al*., 2012; *Rychkov et al*., 2012]. Water surface elevations were modeled using a simple GIS routine. This involved constructing orthogonal channel sections at 5 m streamwise intervals along each wetted anabranch. The water-edge elevation on either side of the channel was then estimated by searching the TLS point cloud at the end of each section. The lowest of the pair of elevations was taken to provide a horizontal estimate of the cross-channel water surface elevation. The 5 m samples were then interpolated streamwise using a channel-based coordinate system to give a continuous water surface elevation model. Whilst generalizing the water surface, this approach mitigates the generation of interpolation artifacts that occur when water surface elevations are incorrectly estimated from the top of cutbanks. Channel bed level elevations were calculated by subtracting an optical-empirical model of water depth from the water surface model. Depths were derived from a set of georeferenced, nonmetric aerial photographs and a calibration depth sounding survey. An optical-empirical model derived from a logarithmic transformation of the ratio of the blue and red band imagery was found to give the optimal fit to the observed depth soundings. The exposed and bathymetric models were fused to generate a 0.5 m resolution DEM (Figure 5b) that has an estimated vertical mean error (ME; Table 2) and a standard deviation of error (SDE) of −0.008 and 0.007 m, respectively, for the

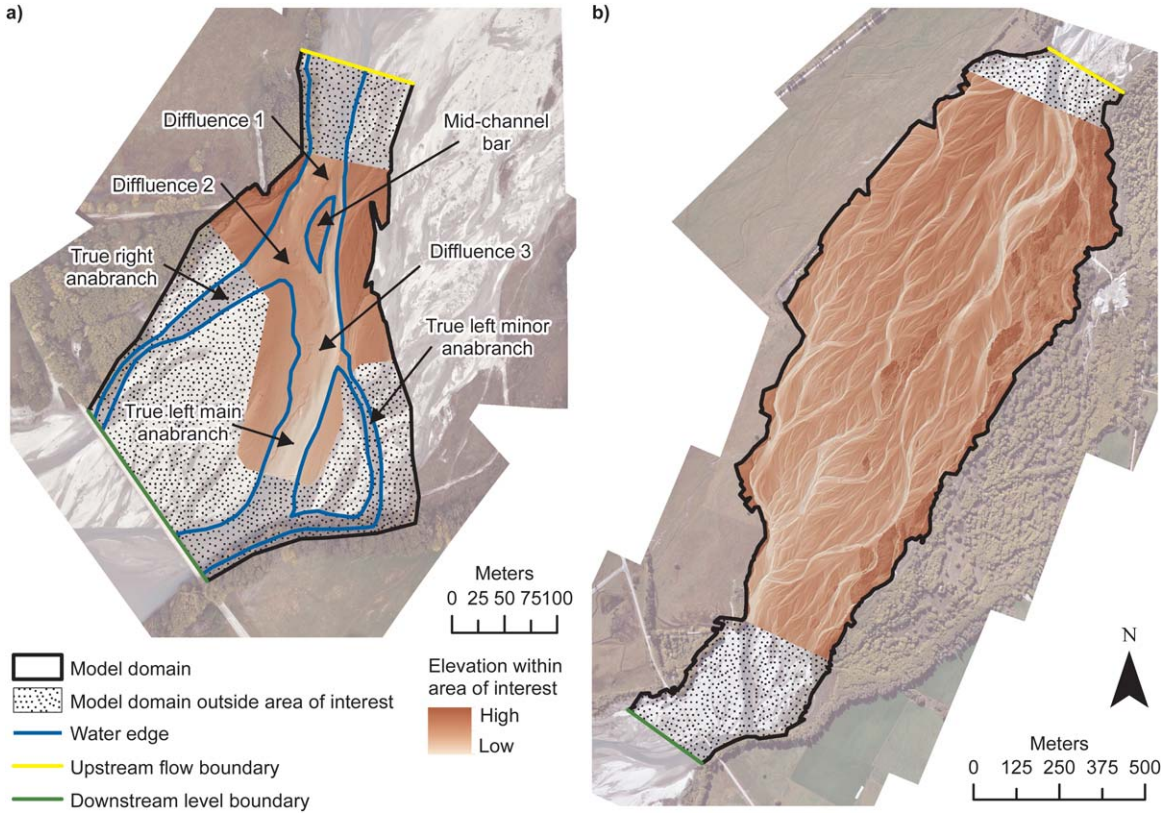

Figure 5. DEM and model schematics for (a) partial braid bar unit (mesoscale) and (b) braided (macroscale) reach. The DEM for the partial braid bar unit is for survey B. The braided (reach-scale) DEM has been detrended of longitudinal slope to improve visualization.

exposed braidplain topography, and a ME and SDE of 0.025 and 0.089 m, respectively, for the inundated channel bed level. Overall, the exposed braidplain topography has low bias and is precise, although errors are likely to be spatially variable and related to morphology [*Heritage et al*., 2009; *Milan et al*., 2011]. The inundated component of the DEM also has low bias, but the variability of error is comparatively high as a consequence of the less precise remote-sensing technique that is utilized to map the bathymetry.

Table 2. Error Statistics Used to Compare Observed and Simulated Flow Dynamics (Depth and Depth-Averaged Velocity)[a]

Error Statistic	Formula
Mean error	$ME = \frac{\sum_i^n (x_{mod} - x_{obs})}{n}$
Standard deviation of error	$SDE = \sqrt{\frac{\sum_i^n ((x_{mod} - x_{obs}) - ME)^2}{n-1}}$
Mean absolute error	$MAE = \frac{\sum_i^n \lvert x_{mod} - x_{obs} \rvert}{n}$
Root mean square error	$RMSE = \sqrt{\frac{\sum_i^n (x_{mod} - x_{obs})^2}{n}}$

[a] x_{obs} is an observed depth or depth-averaged velocity. x_{mod} is a simulated depth or depth-averaged velocity.

3.2.2. Low-Flow Observations: Inundation Extent, Depth, and Velocity

[22] The data acquired to map water depth for the reach-scale DEM are used in this paper to validate low-flow numerical simulations and thus warrant further examination. As reported in *Williams et al*. [2013], a 0.2 m resolution aerial image of the braidplain was constructed by georeferencing and mosaicking a set of seven aerial photographs, using at least 15 control points per image. These aerial photos were taken on 10 April 2010, at a discharge of 7.3 m^3 s^{-1}. A set of 15 independent check points indicate the mosaicked aerial image has a root mean square error (RMSE) of 0.85 m. A manually supervised classification of the inundation extent shown on the image was not possible due to difficulties discriminating between exposed wet gravel and shallow channels. The inundation extent was therefore digitized manually. Whilst georeferencing and manual digitizating introduce errors [*Hughes et al*., 2006], these were constrained by corroborating the results with the TLS point cloud, which as the sensor is not water penetrating records no data returns in wet alreas.

[23] A Sontek S5 RiverSurveyor aDcp was used to measure depth and velocity along zigzag transects in primary anabranches (Figure 2d). This survey was completed immediately after aerial photos were acquired and flow was steady during this period. The S5 aDcp was configured and operated in a similar manner to the M9 aDcp used for the partial braid bar unit measurements, as described above,

although the aDcp was mounted on a Sontek Hydroboard. A total of 5285 depth samples were acquired; of these, 2927 samples were associated with measured velocity ensembles. Table 3 lists the maximum, mean, and standard deviation statistics for the samples.

3.2.3. High-Flow Observations: Inundation Extent and Discharge

[24] Nonmetric aerial photos of the inundated braidplain were taken from a R22 helicopter flying approximately 1500 m above the braidplain at 13:15 on 22 March 2010, on the falling limb of the 323 $m^3\ s^{-1}$ high-flow event. Eight aerial photos providing complete coverage were selected and georeferenced by matching objects in the photos with corresponding survey points in the TLS point cloud. At least 15 control points were used to georeference each image using rubber sheeting. The images were mosaicked and resampled to a 0.25 m resolution. A further set of 15 independent check points extracted from the TLS cloud were used to assess the final image quality, which was found to have an RMSE of 0.96 m. This is of a similar magnitude to that estimated for the low-flow imagery. Inundation extent was delimited using a supervised image classification, supplemented by manual digitization in areas of the braidplain that were shaded or obscured by cloud or trees.

4. Numerical Model Simulations and Performance Assessment

4.1. Delft3d

[25] Steady state depth-averaged flow conditions were simulated using the open-source hydrodynamic code Delft3d (Version FLOW4.00.07). This code solves the Navier Stokes equations using shallow water assumptions and the Boussinesq approximation. Delft3d has previously been widely applied to fluvial, estuarine, and oceanic flow and morphological change simulations [e.g., *Kleinhans et al*., 2008; *Rinaldi et al*., 2008; *van der Wegen and Roelvink*, 2008; *van der Wegen et al*., 2008; *Crosato et al*., 2011; *van der Wegen et al*., 2011; *Crosato et al*., 2012]. Delft3d was utilized in a 2-D mode where the effect of secondary flow on river bends is accounted for by extending the momentum equations to account for spiral motion intensity and horizontal effective shear stresses from the secondary flow. The shallow water equations are solved using an alternating direction implicit (ADI) method, and the horizontal advection terms are spatially discretized using a Cyclic method [*Stelling and Leendertse*, 1992]. Further details on the numerical model are available in *Deltares* [2011], *Lesser et al*., [2004], and *van der Wegen and Roelvink* [2008]. Flow equations are formulated using Cartesian orthogonal curvilinear coordinates. An appropriate time step was used to ensure stability according to the Courant-Friedrichs-Levy condition. Each simulation started with model grid cells that were wet along the downstream boundary but dry elsewhere. Flow was gradually increased at the upstream boundary and then kept constant, at the appropriate discharge, until steady state conditions were reached.

Table 3. Flow Dynamics for High-Flow and Low-Flow Braided Reach (Macroscale) Surveys

Discharge, $m^3\ s^{-1}$		54.7 (High)	7.3 (Low)
Date		22 March 2010	10 April 2010
Effective width, We_{obs}, m		176.7	34.5
Inundation area, IA_{obs}, m^2		308,441	60,720
Depth[a], m	Mean	–	0.38
	Standard deviation	–	0.14
	Maximum	–	1.45
Velocity[a], ms^{-1}	Mean	–	1.09
	Standard deviation	–	0.34
	Maximum	–	2.26

[a]From primary anabranch aDcp survey (only undertaken at low discharge).

[26] Model grids with a 2 m resolution were built for both the partial braid bar unit and reach domains using Deltares RGFGRID software. Additional grids ranging in resolution from 1 to 6 m were also built for the partial braid bar unit, for sensitivity testing. The splines of each grid were orientated to approximately the main flow direction. Elevations were assigned to each grid cell by calculating the mean of any topographic points within each cell, using Deltares QUICKIN software. Flow and level boundaries were set at the upstream and downstream limits of the model domain, respectively (Figure 5). The boundaries were positioned sufficiently far away from the areas of interest to mitigate errors in upstream velocity distributions and downstream backwater effects. Each simulation was calibrated with a uniform bed roughness, using the Colebrook-White equation to determine the 2-D Chezy coefficient, C_{2D}:

$$C_{2D} = 18\log_{10}\left(\frac{12H}{k_s}\right) \tag{1}$$

where H is water depth and k_s is the Nikuradse roughness length. k_s is commonly expected to take a factor, α_x, of a characteristic grain diameter, D_x:

$$k_s = \alpha_x D_x \tag{2}$$

[27] In this paper, we take D_x to be the bed surface D_{84} since, compared to the median grain size, D_{50}, it represents the protrusion of larger grains into the flow. A large range of α_x values have been proposed for hydraulic modeling of rivers [*Millar*, 1999; *Garcia*, 2008].

[28] Simulations were also calibrated using a uniform value of horizontal eddy viscosity, ν_H. This parameter incorporates internal fluid flow resistance due to 3-D turbulent eddies and horizontal motions not resolved by the horizontal grid [*Deltares*, 2011]. Relatively little specific guidance was available on suitable horizontal eddy viscosity values. Delft3D uses a drying and wetting algorithm that sets cells as "wet" if the water depth in the cell rises above a user-defined threshold depth of inundation and "dry" if the water depth drops below half of the threshold depth. The threshold depth was set at 0.05 m for all simulations except those simulations that assessed the sensitivity of this parameter at the braided reach (macroscale).

4.2. Experimental Framework

[29] A two-phase experimental framework is used for model calibration and validation. First, simulations are parameterized at the partial braid bar unit (mesoscale).

Second, model domains are upscaled, with the same cell sizes, to the braided reach (macroscale) to assess whether the parameterization is valid. This framework is based on making the maximum utility of dense observations on flow dynamics available at the mesoscale and using these to inform the parameterization of a macroscale model, where observations are sparser yet where model results are more directly relevant to the scales of river management.

[30] Figure 1 details the experimental framework. At the braid bar unit (mesoscale), spatially dense high-flow observations are used to calibrate the model by varying bed roughness and horizontal eddy viscosity (Simulation A). The sensitivity to grid resolutions, Δx, and the variation in discharge gauged at the upstream end of the unit is then examined. Next, the calibrated parameters are applied to medium-flow and low-flow simulations (B and C), and a sensitivity analysis is undertaken to assess the impact of small changes in bed roughness and horizontal eddy viscosity.

[31] At the braided reach (macroscale), the calibration is transferred to low-flow and high-flow simulations that are undertaken at a greater spatial extent, with the same grid resolution. Model sensitivity is tested by varying bed roughness, inflow discharge, and minimum flow depth. The upscaling of the models is inevitably associated with a relative decrease of instream flow observations that are available to support validation. At this scale therefore, the assessment of predictive performance is supported by comparison with observed inundation extent.

4.3. Performance Assessment

4.3.1. Depth and Velocity

[32] Predicted depths and velocities were compared to aDcp observations for the braid bar unit (simulations A, B, and C) and the braided reach low-flow simulations. For the braid bar unit experiments, the mean and standard deviation depth and velocity observations were calculated for each model grid cell that contained at least three observations. Grid cells with less than three observations were discarded from the performance analysis. This criterion was necessary to alleviate the difficulties in comparing point observations with spatially average predictions and to average turbulent fluctuations and single ping aDcp errors associated with velocity measurements [cf., *Rennie and Church*, 2010]. The standard deviation of aDcp depth, SD_d, and velocity, SD_v, observations were calculated for all model grid cells with at least three aDcp observations. This was used to quantify variability in observed depth and velocity observations in each model grid cell.

[33] Predicted and observed depths and velocities were compared by calculating the mean error (ME), standard deviation of error (SDE), mean absolute error (MAE), and root mean square error (RMSE), as defined in Table 2. The cumulative distributions of depth and velocity errors were also plotted for each set of experiments.

4.3.2. Inundation Extent

[34] The routing of flow across braidplains is strongly influenced by subtle variations in topography. This results in heterogeneous distributions of flow across a reach, with multiple diffluence and confluence units. When viewed in plan, the complex routing of flow provides an opportunity to evaluate model performance, since errors in flow routing at diffluences are likely to generate relatively significant errors in the areal extent of inundation.

[35] Two performance assessments are used to compare observed, IA_{obs}, and predicted, IA_{mod}, inundation areas for flow simulations at the braided reach scale. The first assessment uses a measure of the effective width, We:

$$W_e = \frac{IA}{L} \tag{3}$$

where IA is inundation area and L is river length. This yields a reach-averaged width and is the equivalent of using an infinite number of cross sections to measure water surface width [*Smith et al*., 1996; *Ashmore and Sauks*, 2006]. The performance assessment is then based on the ratio of the predicted, We_{mod}, and observed, We_{obs}, effective widths, respectively:

$$Fit_{We} = \frac{We_{\mathrm{mod}}}{We_{obs}} \tag{4}$$

[36] A more stringent performance assessment [*Bates and De Roo*, 2000] tests whether the areal extents of observed and modeled inundation (IA_{obs} and IA_{mod}) are congruent with one another:

$$Fit_{congruent} = \frac{IA_{obs} \cap IA_{\mathrm{mod}}}{IA_{obs} \cup IA_{\mathrm{mod}}} \tag{5}$$

[37] Whilst this measure may not discriminate uniquely between observed and modeled inundation extents in topographically confined floodplains, it is a very useful performance assessment for braided rivers where flows are relatively shallow and flow routing is complex. For both measures of fit, modeled inundation areas were mapped directly from grids of predicted wet cells. Table 3 lists IA_{obs} and We_{obs} for high-flow and low-flow observations.

5. Results

5.1. Partial Braid Bar Unit (Mesoscale)

5.1.1. Calibration (Simulation A)

[38] Simulation A is assessed using aDcp data that were acquired during relatively high flow (35.6 m^3 s^{-1}), when the midchannel bar within the survey unit was completely inundated. At the time of survey, flow entered the unit through a single channel approximately 40 m wide, before dividing (diffluence 1 on Figure 5a) around the bar. Downstream of this diffluence, the true left anabranch was narrow and deep, whilst the true right anabranch was wider and relatively shallow. Flow in the true right anabranch divided at diffluence 2 (Figure 5a), although the true right anabranch was shallow, with a depth of <0.25 m during the highest flow survey. The anabranches around the bar met at a confluence unit immediately downstream of the bar, with an angle of approximately 35°. Flow was then confined to a single channel with a width of up to 30 m, although some discharge flowed down a minor anabranch (diffluence 3 on Figure 5a). The aDcp survey transects extended across the full width of the unit, and the subsequent depth and velocity data were used to calibrate the numerical model by varying horizontal eddy viscosity and bottom friction.

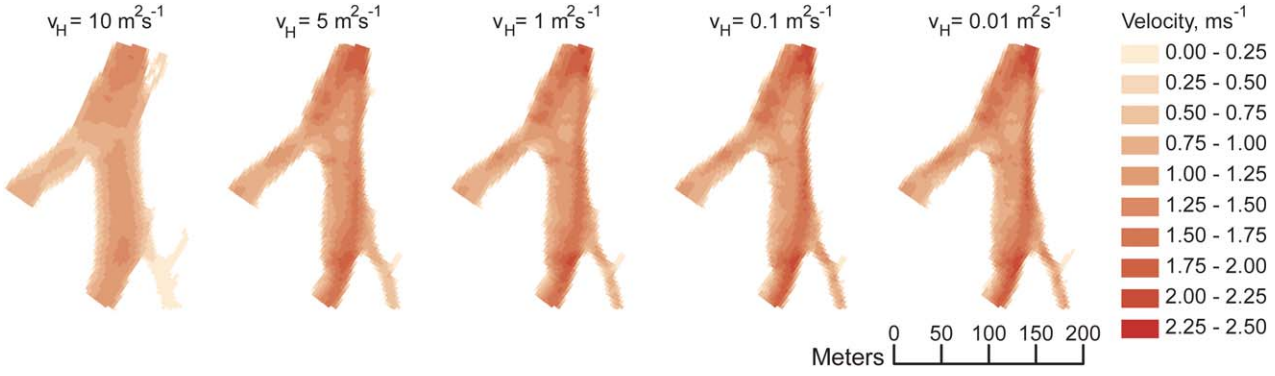

Figure 6. Simulated depth-averaged velocity for partial braid bar unit simulation A, for different horizontal eddy viscosity values, m^2 s^{-1}, as indicated above each map ($k_s = 0.08$ m, $\Delta x = 3$ m). Error measures are listed in Tables 4 and 5.

[39] A wide range of values have been estimated for the ratio, α_x, between the Nikurdse roughness length and D_{84} [*Garcia*, 2008]. Based on previous experience, bed roughness was initially set to $2.3D_{84}$, so $k_s = 0.08$ m. Horizontal eddy viscosity was calibrated using values from 0.01 to 10 m^2 s^{-1}. Figure 6 shows maps of simulated depth-averaged velocity for each horizontal eddy viscosity value. Overall, velocities become more spatially uniform in both longitudinal and transverse flow directions as horizontal eddy viscosity was increased. The primary high velocity flow pathway, along the true left of the braid bar unit, is considerably more longitudinally coherent for the simulations where $\nu_H = 0.1$ and 0.01 m^2 s^{-1}. Horizontal eddy viscosity also influences flow routing (Table 4), with the simulation where $\nu_H = 10$ m^2 s^{-1} poorly representing the flow pathway down the true left minor anabranch. Table 5 compares predicted depths and velocities to those measured using the aDcp, and Figure 7 shows the cumulative frequency error distributions. The simulations where $\nu_H = 10$ and 1 m^2 s^{-1} considerably overestimate depth and underestimate velocity relative to the other simulations. The errors for simulations where $\nu_H = 0.1$ and 0.01 m^2 s^{-1} are similar to each other. For these two simulations, the distribution of modeled depth errors is similar to the aDcp depth variation, SD_d, whilst the distribution of modeled velocity errors is slightly higher than the observed aDcp velocity variation, SD_v.

[40] After a suitable representation of velocity variation had been obtained, the model was calibrated for bed roughness, using the same grid resolution. The initial horizontal eddy viscosity calibration simulations indicated that depth was overestimated and velocity was underestimated, indicating that bed roughness needed to be reduced. The Nikuradse roughness length was therefore varied in 0.01 m

Table 4. Anabranch Flow Routing for Partial Braid Bar Unit (Mesoscale) Simulation A[a]

					Anabranch Discharge, m^3 s^{-1}		
Experiment	Inflow, m^3 s^{-1}	Δx, m	ν_H, m^2 s^{-1}	k_s, m	TR	TL Main	TL Minor
Observed	–	–	–	–	8.0 ± 1.4	23.8 ± 0.4	3.8 ± 1.2
Eddy viscosity	35.6	3	10	0.08	8.56	24.92	1.77
			1		8.22	24.00	3.38
			0.5		8.23	23.96	3.41
			0.1		8.28	23.75	3.57
			0.01		8.34	23.72	3.54
Bed friction	35.6	3	0.1	0.08	8.28	23.75	3.57
				0.05	8.43	23.64	3.53
				0.04	8.45	23.88	3.27
				0.03	8.50	23.78	3.31
Inflow	34.7	3	0.1	0.04	8.23	23.49	3.02
	35.6				8.45	23.88	3.27
	36.5				8.67	24.23	3.59
Spatial resolution	35.6	1	0.1	0.04	7.88	23.93	3.69
		2			8.16	23.60	3.73
		3			8.45	23.88	3.27
		4			8.54	23.70	3.35
		5			8.57	23.83	3.20
		6			8.82	23.84	2.94

[a]Figure 5 shows the location of the TR, TL main, and TL minor anabranches.

Table 5. Depth and Velocity Error Statistics for Partial Braid Bar Unit (Mesoscale) Simulation A[a]

					Depth						Depth-Averaged Velocity				
Experiment	Inflow, $m^3\ s^{-1}$	Δx, m	ν_H, $m^2\ s^{-1}$	k_s, m	ME, m	SDE, m	RMSE, m	MAE, m	aDcp SD_d, m	n	ME, ms^{-1}	SDE, ms^{-1}	RMSE, ms^{-1}	MAE, ms^{-1}	aDcpSD_v, ms^{-1}	n
Eddy viscosity	35.6	3	10	0.08	0.16	0.06	0.17	0.16	0.05	764	−0.49	0.46	0.67	0.57	0.18	555
			1		0.06	0.05	0.08	0.07	0.05		−0.19	0.36	0.40	0.32	0.18	
			0.5		0.04	0.05	0.07	0.05	0.05		−0.15	0.33	0.36	0.28	0.18	
			0.1		0.04	0.05	0.06	0.05	0.05		−0.12	0.30	0.32	0.25	0.18	
			0.01		0.04	0.05	0.06	0.05	0.05		−0.12	0.30	0.32	0.25	0.18	
Bed friction	35.6	3	0.1	0.08	0.04	0.05	0.06	0.05	0.05	764	−0.12	0.30	0.32	0.25	0.18	555
				0.05	0.02	0.05	0.05	0.04	0.05		−0.05	0.32	0.32	0.23	0.18	
				0.04	0.00	0.05	0.05	0.04	0.05		−0.02	0.33	0.33	0.23	0.18	
				0.03	−0.01	0.05	0.05	0.03	0.05		0.03	0.34	0.34	0.23	0.18	
Inflow	34.7	3	0.1	0.04	0.00	0.05	0.05	0.04	0.05	764	−0.04	0.33	0.33	0.23	0.18	555
	35.6				0.00	0.05	0.05	0.04	0.05		−0.02	0.33	0.33	0.23	0.18	
	36.5				0.01	0.05	0.05	0.04	0.05		0.00	0.33	0.33	0.23	0.18	
Spatial resolution	35.6	1	0.1	0.04	0.00	0.04	0.04	0.03	0.02	1063	−0.03	0.24	0.24	0.18	0.14	768
		2			0.00	0.04	0.04	0.03	0.04	1252	0.00	0.26	0.26	0.19	0.15	936
		3			0.00	0.05	0.05	0.04	0.05	833	−0.02	0.33	0.33	0.23	0.18	614
		4			0.00	0.07	0.07	0.04	0.06	559	−0.03	0.36	0.36	0.26	0.20	412
		5			0.00	0.09	0.09	0.06	0.06	399	−0.04	0.43	0.43	0.31	0.21	300
		6			0.00	0.09	0.09	0.06	0.07	294	−0.07	0.46	0.47	0.34	0.23	232

[a]Error statistics are defined in Table 2. Model predictions are compared to observations for each model grid cell with at least three aDcp observations; n = total number of grid cells used in comparison.

increments from 0.03 to 0.05 m. This k_s range equated to $\sim 0.9D_{84}$ to $\sim 1.4D_{84}$. Figure 7 shows cumulative frequency error distributions, and Tables 4 and 5 detail the error analysis and anabranch discharges, respectively. As expected, reducing bed roughness corresponds to lower flow depths and higher velocities. The comparison of measured and predicted velocities indicates that $k_s = 0.04$ m gives the best model performance, with a mean error close to 0.00 m for depth and 0.02 ms^{-1} for velocity. The spatial distribution of depth and depth-averaged velocity mean errors for this parameterization are shown in Figure 8. The predictions are relatively precise, especially when taken in the context of a mean observed depth of 0.54 m and velocity of 1.65 ms^{-1}, and the grid-based aDcp observation variation of 0.05 m and 0.18 ms^{-1} for SD_d and SD_v, respectively. For $k_s = 0.04$ m, the routing of flow down the true right anabranch is slightly overpredicted and that down the true left minor anabranch is under predicted, but the magnitudes of the difference are less than the standard deviation errors associated with the anabranch discharge measurements.

[41] The sensitivity of the calibrated simulation, where $\nu_H = 0.1\ m^2\ s^{-1}$ and $k_s = 0.4$ m, was tested with respect to uncertainty in the upstream inflow discharge and the grid resolution. The inflow discharge was varied by one standard deviation of the gauged discharge, as listed in Table 1. The results (Figure 7 and Tables 4 and 5) indicate that varying the inflow by one standard deviation of the gauged upstream flow results in changes to the depth and velocity mean errors that are similar to varying the bed friction by an increment of $k_s = 0.01$ m.

[42] Figure 9 shows depth predictions for simulations across a range of grid sizes from 1 to 6 m. Depth prediction patterns remain remarkably coherent across all the simulations, with relatively little erroneous variation in grid values at adjacent cells as grid size is increased. The error analysis (Table 5) indicates that the depth ME is close to zero for all the grid sizes considered. However, SDE, RMSE, and MAE all increase with increasing grid size. Compared to depth, predicted velocities are far more sensitive to grid size. There is negative bias in all the simulations, although the ME for the 2 m resolution simulation is close to zero. As grid size is increased, the variability of velocity errors increases at a faster rate than the corresponding aDcp velocity variation, SD_v, indicating a loss of precision that is associated with increasing grid size. In terms of flow routing (Table 4), the true left minor anabranch is most sensitive to increases in grid size since the channel's bed topography is increasingly poorly represented in coarser grids. Overall, the depth, velocity, and flow routing error analysis indicates that the model reaches optimum performance at a 2 m grid size.

5.1.2. Testing Calibration (Simulations B and C)

[43] Flow observations for simulations B and C were acquired at medium (23.6 $m^3\ s^{-1}$) and low (14.4 $m^3\ s^{-1}$) flows, respectively. For survey B, the midchannel bar was exposed in-between chutes on the true left of the bar and due to a slug of sediment being deposited, only negligible discharge was routed down the true right minor anabranch. For survey C, the midchannel bar was exposed and there was no flow routed down the true right minor anabranch. Flow models were built using the topographic and inflow data from each survey and a 2 m resolution grid. Based on

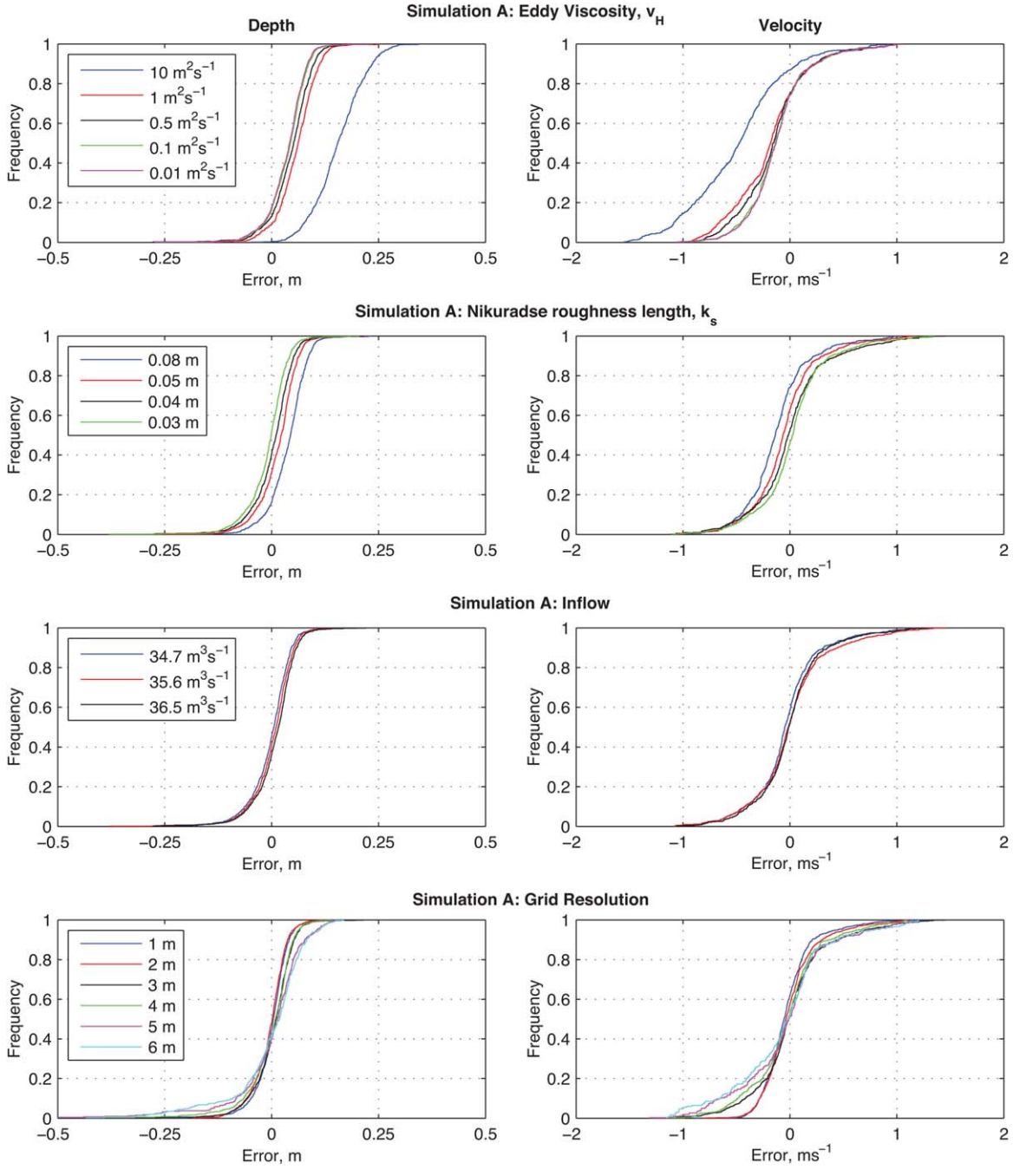

Figure 7. Cumulative frequency error distributions for partial braid bar unit simulation A for calibration by (a) eddy viscosity and (b) bed roughness and sensitivity to (c) discharge and (d) grid resolution. Error measures are listed in Tables 4 and 5.

the findings from simulation A, each model was initially parameterized using $k_s = 0.04$ m and $\nu_H = 0.1$ m^2 s^{-1}. A sensitivity analysis was then undertaken to determine whether a similar optimal parameterization to that found for simulation A was obtained.

[44] For simulation B, the sensitivity test for bed friction (Figure 10 and Table 6) indicates that the mean error for depth is lowest when $k_s = 0.03$ m but mean error for velocity is lowest when $k_s = 0.05$ m. For simulation C, the mean errors for depth and velocity are both lowest when $k_s = 0.03$ m. Importantly, however, the distribution of errors remains similar across the bed friction values tested and the magnitude of variation in depth and velocity mean errors are similar to that calculated for the same range of bed roughness values assessed for simulation A. The spatial distribution of mean errors (Figure 8) is spatially coherent. For example, depth is under predicted on the true left anabranch downstream of diffluence 1 (Figure 5a).

[45] The magnitude of errors calculated by varying the horizontal eddy viscosity for simulations B and C (Figure 10 and Table 6) is also similar to those calculated for the same range of horizontal eddy viscosity values from

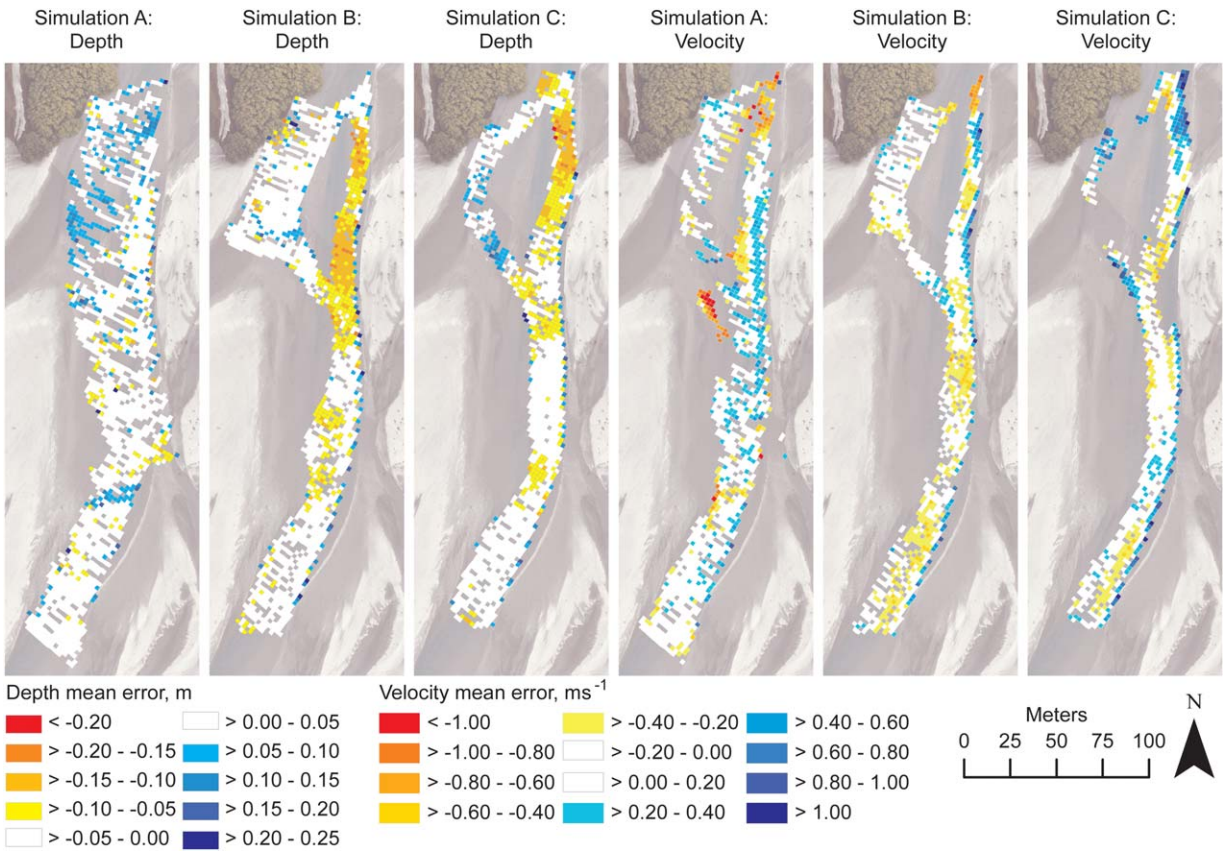

Figure 8. Spatial variation of depth and depth-averaged velocity mean error (ME), for partial braid bar unit (mesoscale) simulations A, B, and C. Mean aDcp measured depth or velocity was calculated for each model grid cell that contained at least three observations. This was then compared to model predictions. Grid cells with less than three observations were therefore discarded from the performance analysis. Mean errors shown are for simulations with $\nu_H = 0.1$ m^2 s^{-1}, $k_s = 0.04$ m, and $\Delta x = 2$ m.

simulation A. Overall, considering the errors from simulations B and C, $\nu_H = 0.01$ m^2 s^{-1} yields the lowest errors. Since the errors for $\nu_H = 0.1$ and 0.01 m^2 s^{-1} for simulation A were similar, the overall optimum value for horizontal eddy viscosity was 0.01 m^2 s^{-1}.

5.2. Braided Reach (Macroscale)

5.2.1. Low-Flow Simulation

[46] Reach-scale, low-flow simulations were undertaken for a discharge of 7.3 m^3 s^{-1}. Based on the results of the calibration experiments described above, the simulations used a grid resolution of 2 m and $\nu_H = 0.01$ m^2 s^{-1}. A bed friction sensitivity analysis was undertaken using k_s values of 0.03–0.06 m, in 0.01 m increments. Figure 11 and Table 7 present an error analysis based on a comparison between simulation predictions and aDcp measurements. Compared to the mean error achieved for the partial braid bar unit surveys, the low-flow simulations consistently overestimate depth, albeit by only 3 cm for $k_s = 0.04$ m. This bias is deemed acceptable when considering the error in the

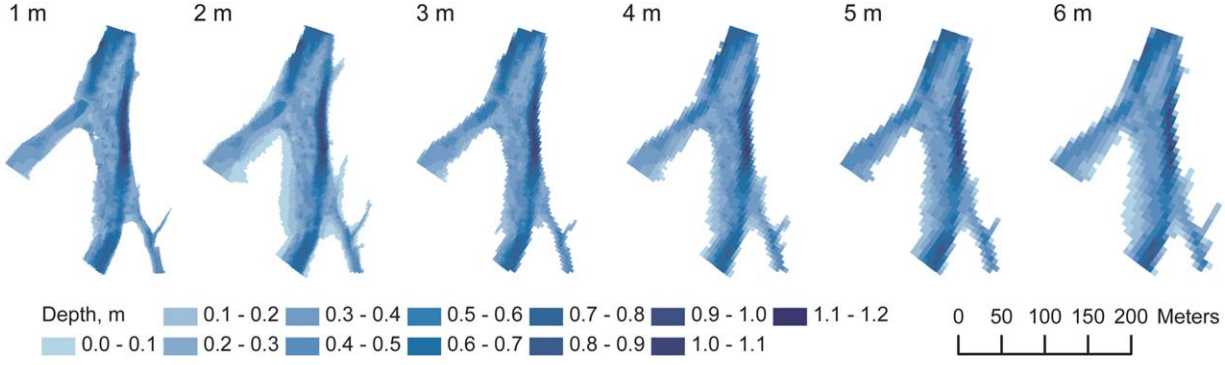

Figure 9. Predicted depths for partial braid bar unit simulation A, for different grid resolutions, as indicated above each map ($\nu_H = 0.1$ m^2 s^{-1} and $k_s = 0.04$ m). Error measures are listed in Tables 4 and 5.

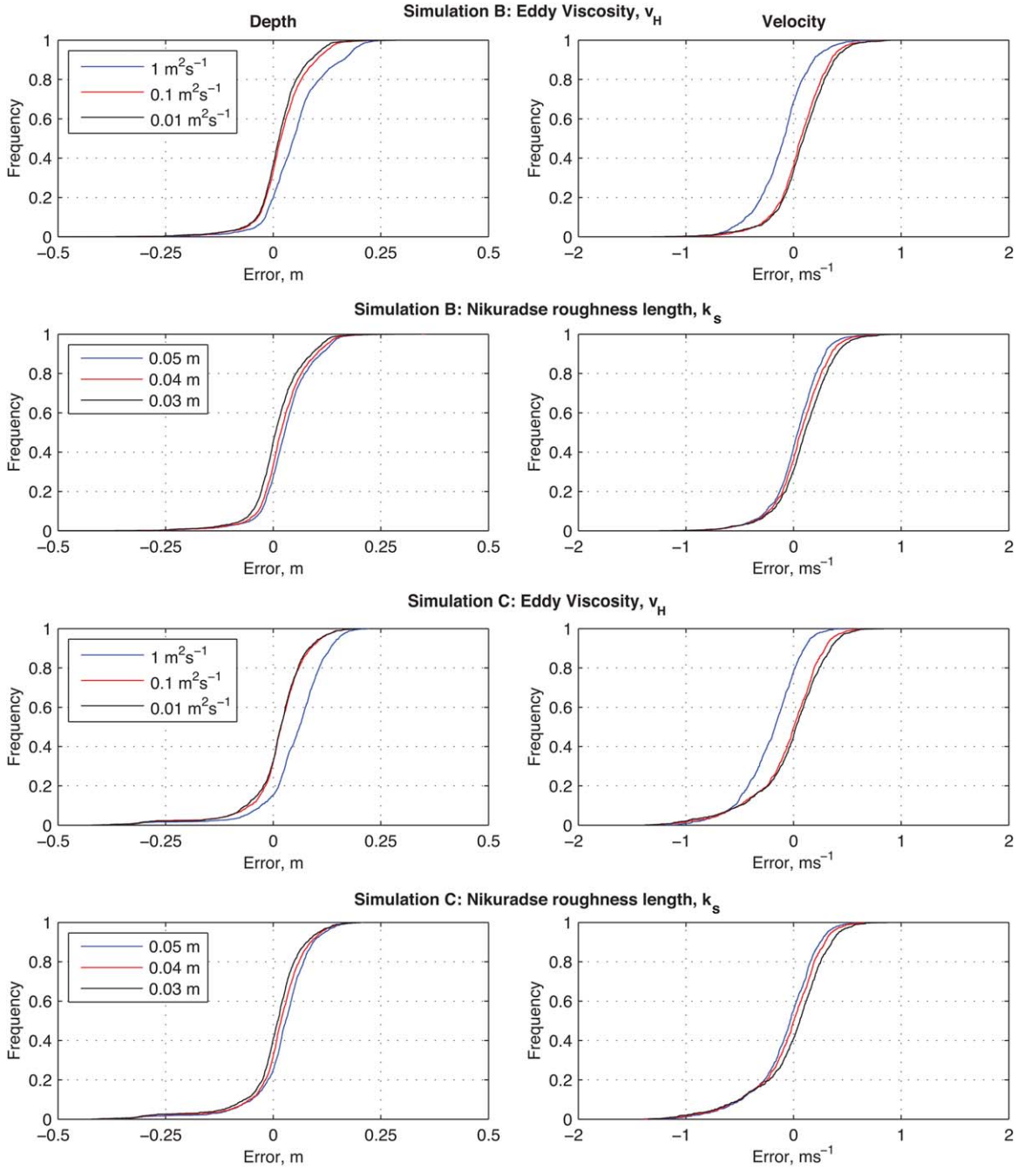

Figure 10. Cumulative frequency error distributions for partial braid bar unit sensitivity analyses for simulations B and C. Error measures are listed in Table 6.

braidplain topographic survey and the different scale of spatial averaging between the computational model grid and the footprint of the aDcp sounding. The magnitude of the velocity mean errors are 0.02 and −0.01 m for $k_s = 0.04$ and $k_s = 0.05$ m, respectively. The magnitudes of the velocity mean errors are similar across the three bed friction values tested and are comparable to the best calibrations for the partial braid bar unit simulations. For both depth and velocity, the variability of error magnitudes are similar to those calculated for the braid bar unit simulation C.

[47] Table 8 shows the inundation extent performance assessments for the low-flow simulations. The Fit_{We} measures range from 131.4 to 135.7%, for k_s values from 0.03 to 0.06 m, respectively. This indicates that predicted inundation extents are consistently greater than those observed. This corresponds to the positive depth mean error that was calculated from the aDcp data. The best congruent inundation extent fit, of 66.1%, is found for $k_s = 0.05$ m. Figure 12a shows the observed and simulated inundation extents for this optimum calibration. Predicted bed shear stresses are shown in Figure 12c. The areal extents of inundation are worthy of further examination since the areal extent fits indicate that there is some disparity between simulation predictions and observations. Simulation predictions,

Table 6. Depth and Velocity Error Statistics for Partial Braid Bar Unit (Mesoscale) Simulations B and C ($\Delta x = 2$ m)[a]

					Depth						Depth-Averaged Velocity				
Simulation	Experiment	Inflow, $m^3\ s^{-1}$	ν_H, $m^2\ s^{-1}$	k_s, m	ME, m	SDE, m	RMSE, m	MAE, m	aDcp SD_d,m	n	ME, ms^{-1}	SDE, ms^{-1}	RMSE, ms^{-1}	MAE, ms^{-1}	aDcpSD$_v$, ms^{-1}	n
B	Bed friction	23.6	0.1	0.03	0.01	0.06	0.06	0.04	0.04	1578	0.10	0.26	0.28	0.22	0.23	1135
			0.1	0.04	0.02	0.06	0.07	0.05	0.04		0.06	0.25	0.26	0.20	0.23	
			0.1	0.05	0.03	0.06	0.07	0.05	0.04		0.03	0.24	0.24	0.18	0.23	
			0.01	0.04	0.02	0.06	0.06	0.04	0.04		0.08	0.27	0.28	0.21	0.23	
	Eddy viscosity		0.1	0.04	0.02	0.06	0.07	0.05	0.04		0.06	0.25	0.26	0.20	0.23	
			1	0.04	0.05	0.07	0.09	0.07	0.04		−0.11	0.25	0.27	0.21	0.23	
C	Bed friction	14.4	0.1	0.03	0.00	0.08	0.08	0.05	0.03	1329	−0.01	0.35	0.35	0.26	0.19	946
			0.1	0.04	0.01	0.08	0.08	0.05	0.03		−0.05	0.33	0.33	0.24	0.19	
			0.1	0.05	0.02	0.07	0.08	0.06	0.03		−0.08	0.30	0.31	0.23	0.19	
	Eddy viscosity		0.01	0.04	0.01	0.07	0.08	0.05	0.03		−0.03	0.35	0.35	0.25	0.19	
			0.1	0.04	0.01	0.08	0.08	0.05	0.03		−0.05	0.33	0.33	0.24	0.19	
			1	0.04	0.05	0.08	0.09	0.08	0.03		−0.21	0.27	0.34	0.26	0.19	

[a]Error statistics are defined in Table 2. Model predictions are compared to observations for each model grid cell with at least three aDcp observations; n = total number of grid cells used in comparison.

assessed by the extent of wetted channel widths, are good where flow is confined to a single channel or relatively wide anabranches but poorer in regions of the braidplain that are characterized by more intense braiding and narrower anabranches. The relatively poorer performance of the simulation in predicting flow along narrow anabranches is particularly evident in the lower, true right region of the reach where inundated channel width is consistently overestimated. This region of the reach contributes to a significant proportion of the areal extent errors and the depth mean error. Indeed, the depth mean error for aDcp samples taken between positions A and B in Figure 12a is 0.07 m. Also, between these positions, mean observed and modeled anabranch widths were 6.4 and 12.6 m, respectively. Thus, at low flow, there is a discrepancy in model performance between narrow and wide anabranches. This may be a consequence of two factors. First, the bed elevation of anabranches with a depth less than 0.25 m are associated with relatively high errors in the DEM because they were below the depth threshold for optical-empirical bathymetric mapping. Second, the resampling of topography first by ToPCAT, to a 0.5 m DEM, and then by QUICKIN, to a 2 m grid for hydraulic modeling, results in topographic smoothing. This causes lower local slope values for the 2 m resolution grid, with particular losses in the cumulative frequency distribution tail for high slopes [*Brasington et al.*, 2012]. The topography responsible for flow steering and form resistance may thus be lost for narrow anabranches. However, high-resolution simulations undertaken using a 1 m resolution grid did not substantially improve the routing of water through the narrow anabranches.

5.2.2. High-Flow Simulation

[48] High-flow simulations were run for a discharge of 54.7 $m^3\ s^{-1}$, using the same topographic boundary conditions as the low-flow simulations. Whilst the braidplain is likely to have undergone some morphological evolution between the acquisition of high-flow aerial photos and topographic data, the primary flow pathways are coherent between the low-flow and high-flow simulations (Figure 12). The predictions from high-flow simulations are thus considered at a broad scale. Table 8 shows the inundation extent performance assessments for simulations with bed friction values of $k_s = 0.04$, 0.05, and 0.06 m. Figure 12b shows the predicted inundation extent for the optimum calibration, where $k_s = 0.05$ m, and Figure 12d shows corresponding predictions of bed shear stress. Across all three of the bed roughness values tested the inundation extents are predicted well compared to the low-flow simulations. The Fit_{We} measure is close to 100% for all the simulations, indicating that the overall extent of inundation is well predicted. However, the $Fit_{congruent}$ measure is lower, with the optimal simulation with $k_s = 0.05$ m yielding a fit of 84.1%. This is consistent with the braidplain topography having morphed between the high-flow aerial photography and the topographic survey. In addition, as was found for the low-flow simulations, predictions of the inundation extent of wider anabranches are better than those for narrower anabranches. Many of these narrow anabranches may, however, have been plugged by deposition by the time topographic data were acquired, as observed by *Rennie et al.* [2012]. Despite this, the overall predicted inundation extent is good considering the

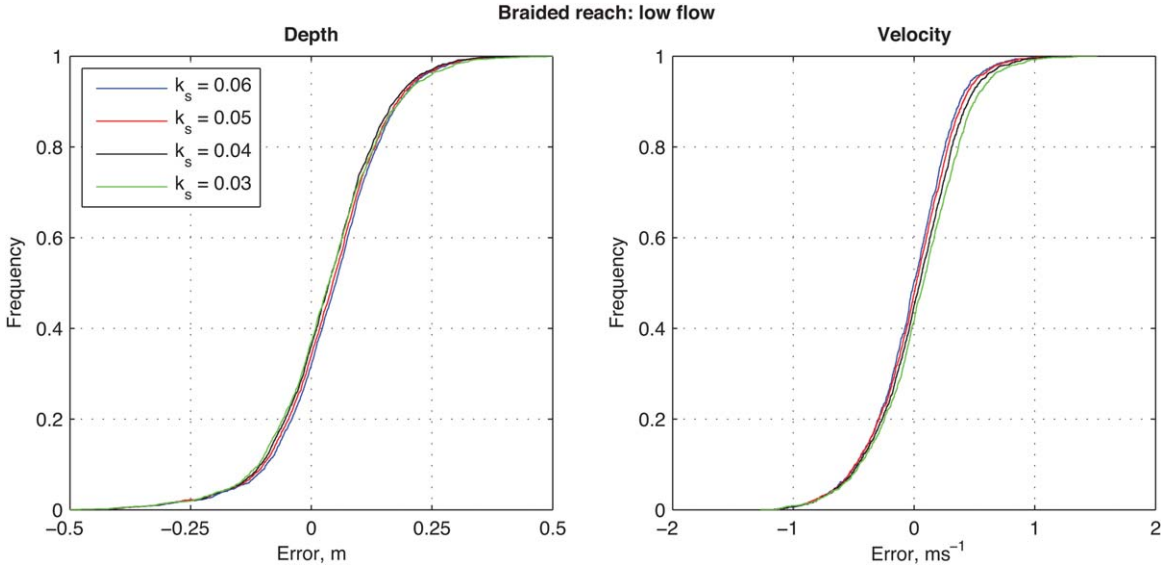

Figure 11. Cumulative frequency error distributions for reach-scale, low-flow (7.3 m^3 s^{-1}) simulation bed roughness calibration. Error measures are listed in Table 7.

relatively low magnitude vertical relief that is characteristic of braidplain morphology.

[49] All the simulations discussed in this paper so far, for both the partial braid bar unit and the braided reach, used a threshold depth (d_{min}) of 0.05 m. To assess the sensitivity of the simulations to this assumption, a set of four simulations were run with the minimum depth of inundation varying from 0.025 to 0.100 m, in increments of 0.025 m. Increasing the threshold depth by an increment of 0.025 m typically increased water levels in the center of anabranches by c.0.01 m and caused depth-averaged velocity to vary by c.0.05 ms^{-1}. Changes in inundation extent were, as would be expected, greater since flow in the shallow margins of the channels is altered (Table 8). For example, reducing the wetting/drying threshold depth to 0.025 increases the predicted inundation area, resulting in a Fit_{We} measure of 113.6%. Conversely, increasing the threshold depth to 0.075 m reduces the predicted inundation area, resulting in a Fit_{We} measure of 86.8%. Whilst there are errors in the digitization of observed inundation areas, it is apparent that the calibration of all the simulations are only valid based upon this threshold being kept constant at 0.05 m. This is physically plausible since the D_{90} grain size of 40.5 mm is likely to inhibit flow in very shallow areas.

6. Discussion

6.1. Calibration Transferability

[50] The results presented in this paper demonstrate that a two-dimensional shallow water model can adequately replicate observed flow dynamics over a gravel-bed, braided river, at a wide range of spatial scales and forcing discharges. Appropriate representation of internal shear stresses, through the parameterization of horizontal eddy viscosity, is shown to be necessary to predict cross-channel variations in depth-averaged velocity. This is critical for simulating braided rivers because high-velocity regions within a braided river network closely correspond to zones of active bedload transport. Correctly simulating lateral velocity distribution is therefore essential in order to use hydraulic predictions as inputs for morphological calculations. The use of instream depth-averaged velocity observations enabled the calibration of horizontal eddy viscosity; it would not have been sufficient to calibrate the model with water level, depth, and inundation extent alone.

[51] Roughness in gravel-bed rivers can arise from sediment grains, grain protrusion, cluster bed forms, dunes, and bar and pool-riffle sequences [*Millar*, 1999]. The acquisition of high-resolution DEMs enables bed topography to be

Table 7. Depth and Velocity Error Statistics for Braided Reach (Macroscale) Low-Flow (7.3 m^3 s^{-1}) Simulations ($\nu_H = 0.1$ m^2 s^{-1}, $\Delta x = 2$ m)[a]

	Depth					Depth-Averaged Velocity				
k_s, m	ME, m	SDE, m	RMSE, m	MAE, m	n	ME, ms^{-1}	SDE, ms^{-1}	RMSE, ms^{-1}	MAE, ms^{-1}	n
0.03	0.02	0.09	0.09	0.04	2456	0.06	0.38	0.39	0.30	1299
0.04	0.03	0.12	0.12	0.09	2456	0.02	0.37	0.37	0.29	1299
0.05	0.04	0.12	0.13	0.10	2456	−0.01	0.36	0.36	0.28	1299
0.06	0.04	0.12	0.13	0.10	2456	−0.02	0.35	0.35	0.27	1299

[a]Error statistics are defined in Table 2. Model predictions are compared to observations for each model grid cell with at least three aDcp observations; n = total number of grid cells used in comparison.

Table 8. Areal Extent Fit for Low-Flow and High-Flow Braided Reach (Macroscale) Simulations ($\nu_H = 0.1$ m^2 s^{-1} and $\Delta x = 2$ m)

Flow, m^3 s^{-1}	k_s, m	Threshold Depth, d_{min}, m	$Fit_{congruent}$, %	Fit_{We}, %
7.3 (low)	0.03	0.050	61.8	131.4
7.3 (low)	0.04	0.050	61.7	133.2
7.3 (low)	0.05	0.050	66.1	133.8
7.3 (low)	0.06	0.050	60.9	135.7
54.7 (high)	0.04	0.050	72.0	97.8
54.7 (high)	0.05	0.050	84.1	100.1
54.7 (high)	0.06	0.050	72.5	100.8
54.7 (high)	0.04	0.100	66.1	79.8
54.7 (high)	0.04	0.075	69.4	86.8
54.7 (high)	0.04	0.050	72.0	97.8
54.7 (high)	0.04	0.025	72.2	113.6

accurately represented in the hydraulic models. The partial braid bar unit (mesoscale) simulations utilize DEMs that were constructed from a fusion of aDcp bathymetric survey and TLS and are characterized by relatively low vertical bias and high vertical precision. Although the aDcp bed level survey points are not as spatially dense as the TLS data, their spatial density is still commensurate with the resolution of modeling being undertaken for this study. DEMs for the reach (macroscale) simulations were constructed from a fusion of empirical-optical bathymetric mapping and mobile TLS, for wet and dry areas of the braidplain, respectively, as described in *Williams et al.* [2013]. Wet alreas are characterized by higher vertical variability of error than dry areas, due to the lower precision of the optical-empirical bathymetric mapping technique, but the mapping technique does ensure spatially extensive mapping. Overall, all DEMs are of a sufficiently high resolution to account for form roughness, which arises from the interaction of flow and bed microtopography. Indeed, the results from varying the spatial resolution of simulation A indicate that selecting a grid resolution that is sufficiently fine to capture form roughness is necessary to minimize velocity errors. Since the bed roughness calibration captures resistance associated with sediment grains and their protrusion, it is interesting to interpret the Nikuradse roughness length in the context of the D_{84} grain size diameter, which represents the protrusion of larger grains into the flow. Considering the optimum calibrations achieved for each of the three flow discharges across the partial braid bar unit, and the low and high discharges through the reach, the scaling factor, α_x (equation (2)), for D_{84} ranges from 1.2 to 1.4. This value is considerably lower than those reported in reviews of investigations that have estimated ratios between the Nikuradse roughness length and characteristic sediment sizes [*Millar*, 1999; *Garcia*, 2008] indicating that the high-resolution model topography used for this study captures more of the form roughness than topography used in previous studies. This finding provides important guidance for similar high-resolution hydraulic modeling investigations of gravel-bed rivers, where form roughness is captured by high-resolution model topography.

[52] Since the calibrated Nikuradse roughness length represents grain roughness and protrusion, it was possible to transfer the calibrations between the different simulations at the partial braid bar unit scales, which all consider relatively shallow river flows. The transfer of best fit parameters from the highest flow partial braid bar unit simulation (simulation A) to medium-flow and low-flow simulations (simulations B and C) yielded similar magnitude errors in depth and depth-averaged velocity

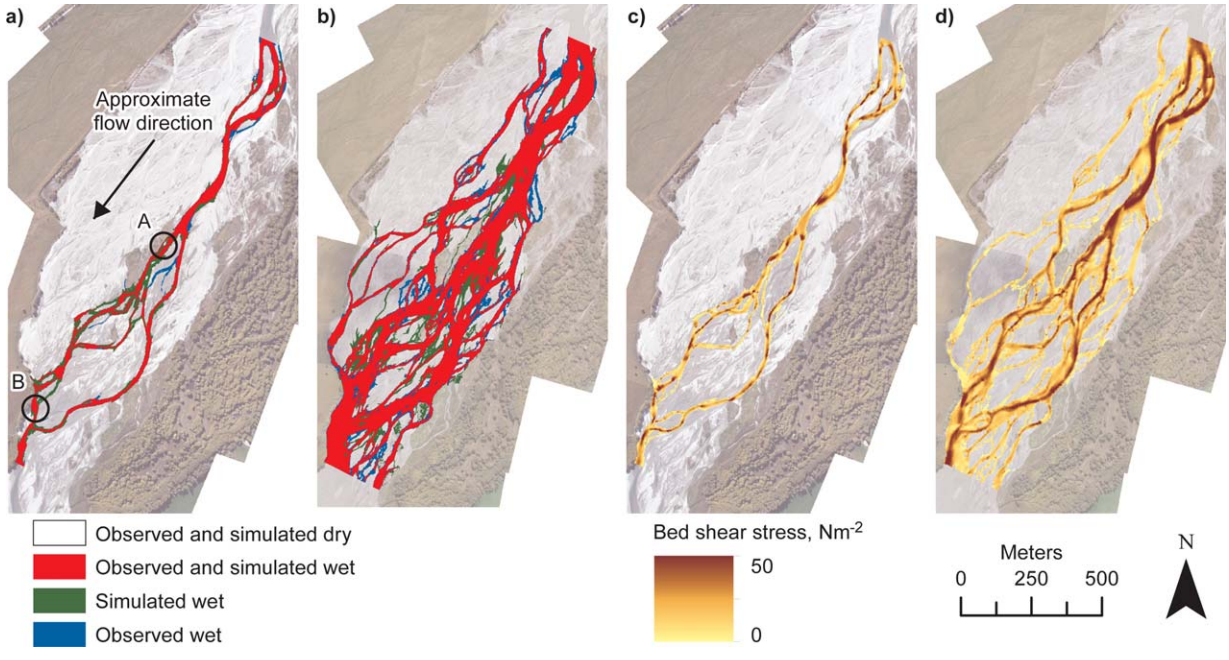

Figure 12. Observed and predicted inundation extents for reach scale (a) low (7.3 m^3 s^{-1}) and (b) high (54.7 m^3 s^{-1}) flows and corresponding predicted bed shear stress for (c) low and (d) high flows. Both simulations use $\nu_H = 0.1$ m^2 s^{-1}, $k_s = 0.05$ m, $\Delta x = 2$ m, and $d_{min} = 0.05$ m. Markers (A) and (B) identify anabranches that are discussed in the text.

predictions. Sensitivity analyses of the horizontal eddy viscosity and bed roughness parameterizations also produced similar error distributions across the high-flow, medium-flow, and low-flow simulations. The SDE between the observed and modeled depths and velocities are typically slightly higher than the variation of aDcp observations (SD_d and SD_v) in each model grid cell. This suggests that variation in model prediction is more likely to be associated with model errors than either observational errors or errors associated with comparing point aDcp observations with gridded hydraulic predictions. The magnitude of the variation is, however, acceptable.

[53] Spatially uniform parameterizations of horizontal eddy viscosity and bed roughness are used for all simulations for two reasons. First, given the labile nature of braided rivers such as the Rees, a central tenet of the assessment was to consider whether constant parameterizations yield adequate predictions. Second, constant parameterizations are usually considered as a starting point for simulating channel morphodynamics. Surface sedimentology of braided rivers varies across a range of scales [*Ashworth and Ferguson*, 1986; *Ashworth et al*., 1992]. Whilst TLS data can be used to map surface roughness of dry areas [*Heritage and Milan*, 2009; *Brasington et al*., 2012], mapping the surface roughness of wet alreas is more challenging, although techniques based upon image processing have been demonstrated [e.g., *Carbonneau et al*., 2005]. For this study, insufficient spatially distributed data were available to map the sedimentology of wet alreas and then assess hydraulic predictions of spatially variable bed roughness parameterizations. However, spatially variable parameterizations of horizontal eddy viscosity and bed roughness may improve model performance, as shown by *Papanicolaou et al*. [2011a] for 2-D simulation of flow around bendway weir structures. In particular, for the Rees River, high roughness close to anabranch banks will create complex shear zones, and spatial variations in grain size distributions will result in variable bed roughness. Within a multisediment fraction morphological model, where sedimentology evolves through time, an interesting sensitivity analysis would be to evaluate the variation in hydraulic predictions based on spatially variable bed roughness based on sediment size and a constant roughness parameterization.

[54] To simulate flow dynamics at the braided reach (macroscale), the optimized parameterization from the partial braid bar unit (mesoscale) was transferred to a larger model domain with a similar grid resolution. In a similar manner to the transfer of the bed roughness calibration for different discharge simulations at partial braid bar unit scale, the calibration could be transferred because it was associated with grain roughness and protrusion. At low flow, adjusting bed roughness to minimize compensating mean errors in depth and velocity resulted in an optimized parameterization that resulted in slight overprediction of flow depth. This bias and the longer tails in error distributions for the braided reach-scale error analysis are likely to be related to inaccuracies in the braided reach DEM. These errors may arise from topographic smoothing due to resampling of surveyed elevations to a coarser computational grid and limitations associated with the minimum depth threshold of 0.25 m for the optical-empirical bathymetric mapping method. The bathymetry of narrow, shallow anabranches is thus poorly represented in the DEM and results in water surface elevations, and hence depths that are higher than observed. Despite this, the performance of the 2-D model in predicting depth, velocity, and inundation extent at low flow is remarkably good. Model performance is also good at high flow, with correct flow routing along the main anabranches. Moreover, the best fit bed roughness parameterization is the same as that for low flow, indicating coherence across change in discharge due to the significant expansion in the aerial extent of flow and the continuation of relatively shallow flow.

6.2. Uncertainty Analysis

[55] The optimized parameterization that is presented for simulating braided river flow is not necessarily unique, and there may be a number of parameter sets that are equally good at predicting flow dynamics [*Beven and Freer*, 2001; *Beven*, 2006]. This concept of equifinality, where there are multiple parameter sets that yield acceptable models, could be explored using a Monte Carlo approach [*Beven and Binley*, 1992; *Spear et al*., 1994; *Beven and Freer*, 2001; *Parker et al*., 2009; *Rye et al*., 2012], on a high performance computing platform, and further assessment of the errors associated with the observational data used to measure model performance. Such an approach is beyond the scope of this paper but the sensitivity analyses reported here nonetheless provide useful guidance on the key parameters and suitable parameter ranges. For example, simulation at the scale of a partial braid bar unit indicates that varying discharge by one standard deviation of the discharge measured at the upstream end of the unit results in changes to depth and velocity errors that are similar to varying bed roughness by $k_s \pm 0.01$ m. For the braided reach high-flow simulations, errors in measuring discharge are likely to be significant, and guidance available in *McMillan et al*. [2012] could be used to select appropriate discharge ranges. Compensating parameterizations associated with changing grid resolution could be fully explored with a Monte Carlo approach. Similarly, the sensitivity of all the simulations undertaken to the threshold depth, as tested in the braided reach high-flow simulation, indicate that there is likely to be a compensatory effect between bed roughness and the threshold depth. This is particularly the case in simulations of braided river flow because even high discharges are characterized by relatively shallow depths, particularly over bar tops.

[56] Uncertainties in model topography also contribute to errors in predicted flow dynamics. In particular, anabranches shallower than 0.25 m are associated with higher errors than deeper anabranches. This is because optical-empirical bathymetric mapping used a calibration data set that did not feature observations of depth <0.25 m due to the minimum measurement capability of the aDcp. Errors in high-resolution surveys of topography are explicitly recognized in techniques applied to estimate morphological sediment budgets [e.g., *Wheaton et al*., 2010]. However, detailed work on assessing the impact of topographic uncertainties on flow simulations have received less attention [*Legleiter et al*., 2011]. These uncertainties could be investigated further by resampling precise, high-resolution survey data such as the ReesScan data set [*Williams et al*., 2013] to produce DEMs of varying resolutions.

Incorporation of grid resolution variation, and stochastically generated DEM errors, into an uncertainty analysis would provide insight into the relationship between the quality of model predictions and the resolution and precision of model topography. This would contribute to understanding the magnitude of topographic error that is acceptable before flow is incorrectly routed at diffluences.

6.3. Applications

[57] Two-dimensional flow models are used for a wide range of applications including predicting flood inundation dynamics, instream habitats, bedload transport, and morphological change. The good model predictions for flow routing, depth and depth-averaged velocity indicate that these models are likely to have utility in providing estimates of shear stress. *Van De Wiel et al*. [2011] suggest that morphodynamic simulations would benefit from a more physically complete representation of flow hydraulics to improve the realism of simulated landscapes. The tradeoff between the physical completeness of hydraulic models and their computational efficiency has recently been examined by *Nicholas et al*. [2012] who compare the performance of reduced-complexity and physically rich models. These authors note that whilst reduced-complexity models are capable of successfully predicting flow depths and velocities, the reduced-complexity approach can produce local flow accelerations in shallow depths. Furthermore, *Nicholas et al*. [2012] note that to complete unsteady simulations, which are necessary for morphodynamic simulations, there is only a marginal gain in computational efficiency when using a reduced-complexity flow routing model compared to a more physically rich model due to the number of iterations that must be made by the reduced-complexity flow routing algorithm at each simulation time step. The results presented herein demonstrate that a 2-D, physically rich numerical model is capable of making realistic hydraulic predictions across a topographically complex river bed. This suggests that using this approach to hydraulics modeling will have utility in morphodynamic simulations.

7. Summary and Conclusions

[58] This paper examines the hydraulic predictions of a two-dimensional shallow water model for simulating braided river flow dynamics using high-resolution data sets of depth and velocity measurements and flood inundation extents. To the authors' knowledge, the DEMs that are used as model boundary conditions and the aDcp surveys that are used for model assessment are of an unprecedented resolution and precision for simulating flow within a natural braided river environment. Two sets of simulations were undertaken. The first set focused on simulating flow dynamics through a 300 m long partial braid bar unit where high-resolution observations of depth and depth-averaged velocity were available from spatially dense aDcp surveys undertaken at three flows. The second set simulated flow dynamics through a 2.5 km long braided reach, using a similar grid resolution to the partial braid bar unit simulations. For the reach-scale simulations, aDcp velocity and depth observations were comparatively sparse and so aerial imagery was also used to assess inundation extent at low and high flows.

[59] Acceptable error distributions in predicted depth and depth-averaged velocity were obtained using spatially constant bed roughness and horizontal eddy viscosity parameter sets. Whilst spatially variable parameterization may reduce errors, further insufficient boundary data were available to investigate this further. Appropriate calibration of horizontal eddy viscosity ($\nu_H = 0.1$ to 0.01 m^2 s^{-1}) was essential to accurately predict cross-channel variations in depth-averaged velocity. This is important if model predictions of braided river flow dynamics are to be used to estimate bedload transport and morphological change. The use of high-resolution DEMs (2 m grid) as boundary conditions for the hydraulic simulations meant that some contribution of form roughness was represented explicitly in the model topography. Calibration of bed roughness therefore represents the smaller-scale effects of grain roughness and protrusion, and particle clusters. The optimum values of the Nikuradse roughness length, k_s, found for each simulation equated to 1.2 to 1.4 D_{84}. These values are lower than those reported for calibrated models that have lower resolution topography. For high-flow, reach-scale simulations, predicted inundation areas were shown to be relatively sensitive to the wetting/drying threshold depth.

[60] The representation of form roughness in high-resolution model topography enabled the transfer of the calibrated bed roughness parameter from the partial braid bar unit to the reach-scale simulations. The flow model was thus calibrated at the partial braid bar unit, where dense instream flow observations were available, and then shown to make good predictions at the reach scale. Both the partial braid bar unit and reach-scale models make relatively effective predictions of flow routing at major diffluences in the anabranch network, when optimum parameter sets are used. Given the relatively low relief and intricate nature of braidplain morphology, the performance of the simulations is good and demonstrates the utility of using accurate, high-resolution DEMs for hydraulic modeling of braided rivers. Overall, the relatively low bias, and acceptable error distributions, of depth and depth-averaged velocities obtained from the simulations suggest that high-resolution, two-dimensional shallow water models are capable of making predictions of braided river flow that are fit for purpose in a range of applications.

[61] **Acknowledgments.** The authors would like to thank Ramon Batalla, Jose López-Tarazón, Becky Goodsell, Jo Hoyle, Helen Reid, Eric Scott and Mark Smith for field assistance. Field campaigns were primarily funded by NERC Grant NE/G005427/1 and NERC Geophysical Equipment Facility Loan 892 as well as NSERC and CFI (Canada) grants to Colin Rennie. Damia Vericat was supported by a Ramon y Cajal Fellowship (RYC-2010-06264) funded by the Spanish Ministry of Science and Innovation during the preparation of this manuscript. Numerical simulations were undertaken during a visit by Richard Williams to NIWA. This visit was funded by the British Hydrology Society and an Aberystwyth University Postgraduate Studentship. Murray Hicks and Richard Measures were funded by NIWA core funding under the Sustainable Water Allocation Programme.

References

Aronica, G., P. D. Bates, and M. S. Horritt (2002), Assessing the uncertainty in distributed model predictions using observed binary pattern information within GLUE, *Hydrol. Processes*, *16*(10), 2001–2016, doi:10.1002/hyp.398.

Ashmore, P., and E. Sauks (2006), Prediction of discharge from water surface width in a braided river with implications for at-a-station hydraulic geometry, *Water Resour. Res.*, *42*, W03406, doi:10.1029/2005wr003993.

Ashworth, P. J., and R. I. Ferguson (1986), Interrelationships of channel processes, changes and sediments in a proglacial braided river, *Geografiska Annaler. Ser. A, Phys. Geogr.*, *68*(4), 361–371.

Ashworth, P. J., R. I. Ferguson, and M. D. Powell (1992), Bedload transport and sorting in braided channels, in *Dynamics of Gravel-Bed Rivers*, edited by P. Billi, R. D. Hey, C. R. Thorne, and P. Tacconi, pp. 497–515, John Wiley, Chichester, U. K.

Bailly, J. S., Y. Le Coarer, P. Languille, C. J. Stigermark, and T. Allouis (2010), Geostatistical estimations of bathymetric LiDAR errors on rivers, *Earth Surf. Processes. Landforms*, *35*(10), 1199–1210, doi:10.1002/esp.1991.

Barton, G. J., R. R. McDonald, J. M. Nelson, and R. L. Dinehart (2005), Simulation of streamflow using a multidimensional flow model for white sturgeon habitat, Kootenai River near Bonners Ferry, Idaho, Rep., 56 pp., U.S. Geol. Surv., Va., Scientific Investigations Report 2005-5230, Reston, Virginia.

Bates, P. D. (2012), Integrating remote sensing data with flood inundation models: How far have we got?, *Hydrol. Processes*, *26*(16), 2515–2521, doi:10.1002/hyp.9374.

Bates, P. D., and A. P. J. De Roo (2000), A simple raster-based model for flood inundation simulation, *J. Hydrol.*, *236*(1–2), 54–77, doi:10.1016/s0022–1694(00)00278-x.

Bates, P. D., M. S. Horritt, G. Aronica, and K. Beven (2004), Bayesian updating of flood inundation likelihoods conditioned on flood extent data, *Hydrol. Processes*, *18*(17), 3347–3370, doi:10.1002/hyp.1499.

Beven, K. (2006), A manifesto for the equifinality thesis, *J. Hydrol.*, *320*(1–2), 18–36, doi:10.1016/j.jhydrol.2005.07.007.

Beven, K., and A. Binley (1992), The future of distributed models: Model calibration and uncertainty prediction, *Hydrol. Processes*, *6*(3), 279–298, doi:10.1002/hyp.3360060305.

Beven, K., and J. Freer (2001), Equifinality, data assimilation, and uncertainty estimation in mechanistic modelling of complex environmental systems using the GLUE methodology, *J. Hydrol.*, *249*(1–4), 11–29, doi:10.1016/s0022–1694(01)00421-8.

Brasington, J. (2010), From grain to floodplain: Hyperscale models of braided rivers, *J. Hydraul. Res.*, *48*(4), 52–53.

Brasington, J., B. T. Rumsby, and R. A. McVey (2000), Monitoring and modelling morphological change in a braided gravel-bed river using high resolution GPS-based survey, *Earth Surf. Processes Landforms.*, *25*(9), 973–990, doi:10.1002/1096–9837(200008)25:9<973::AID-ESP111>3.0.CO;2-Y.

Brasington, J., J. Langham, and B. Rumsby (2003), Methodological sensitivity of morphometric estimates of coarse fluvial sediment transport, *Geomorphology*, *53*(3-4), 299–316, doi: 10.1016/S0169-555X(02)00320-3.

Brasington, J., D. Vericat, and I. Rychkov (2012), Modelling river bed morphology, roughness and surface sedimentology using high resolution terrestrial laser scanning, *Water Resour. Res.*, *48*, W11519, doi:10.1029/2012WR012223.

Bunte, K., and S. R. Abt (2001), Sampling surface and subsurface particle-size distributions in wadable gravel- and cobble-bed streams for analyses in sediment transport, hydraulics, and streambed monitoring, *Gen. Tech. Rep. RMRS-GTR-74*, 428 pp., U.S. Dep. of Agric. For. Serv., Rocky Mountain Res. Stn., Fort Collins, Colo.

Carbonneau, P. E., N. Bergeron, and S. N. Lane (2005), Automated grain size measurements from airborne remote sensing for long profile measurements of fluvial grain sizes, *Water Resour. Res.*, *41*, W11426, doi:10.1029/2005wr003994.

Clifford, N. J., P. J. Soar, O. P. Harmar, A. M. Gurnell, G. E. Petts, and J. C. Emery (2005), Assessment of hydrodynamic simulation results for eco-hydraulic and eco-hydrological applications: A spatial semivariance approach, *Hydrol. Processes*, *19*(18), 3631–3648, doi:10.1002/hyp.5855.

Clifford, N. J., N. G. Wright, G. Harvey, A. M. Gurnell, O. P. Harmar, and P. J. Soar (2010), Numerical modeling of river flow for ecohydraulic applications: Some experiences with velocity characterization in field and simulated data, *J. Hydraul. Eng. ASCE*, *136*(12), 1033–1041, doi:10.1061/(asce)hy.1943–7900.0000057.

Coulthard, T. J., M. G. Macklin, and M. J. Kirkby (2002), A cellular model of Holocene upland river basin and alluvial fan evolution, *Earth Surf. Processes. Landforms.*, *27*(3), 269–288, doi:10.1002/esp.318.

Crosato, A., E. Mosselman, F. Beidmariam Desta, and W. S. J. Uijttewaal (2011), Experimental and numerical evidence for intrinsic nonmigrating bars in alluvial channels, *Water Resour. Res.*, *47*, W03511, doi:10.1029/2010wr009714.

Crosato, A., F. B. Desta, J. Cornelisse, F. Schuurman, and W. S. J. Uijttewaal (2012), Experimental and numerical findings on the long-term evolution of migrating alternate bars in alluvial channels, *Water Resour. Res.*, *48*(6), W06524, doi:10.1029/2011wr011320.

Deltares (2011), *Delft3d-FLOW, a documentation report*, 688 pp., Deltares, Delft, Netherlands.

Di Baldassarre, G., and S. Uhlenbrook (2012), Is the current flood of data enough? A treatise on research needs for the improvement of flood modelling, *Hydrol. Processes.*, *26*(1), 153–158, doi:10.1002/hyp.8226.

Dinehart, R. L., and J. R. Burau (2005), Averaged indicators of secondary flow in repeated acoustic Doppler current profiler crossings of bends, *Water Resour. Res.*, *41*(9), W09405, doi:10.1029/2005wr004050.

Doeschl-Wilson, A. B., and P. E. Ashmore (2005), Assessing a numerical cellular braided-stream model with a physical model, *Earth Surf. Processes. Landforms.*, *30*(5), 519–540, doi:10.1002/esp.1146.

Entwistle, N. S., D. J. Milan, and G. L. Heritage (2010), Biotope mapping using combined LiDAR and acoustic Doppler profiler survey, paper presented at BHS 3rd International Symposium: Managing Consequences of a Changing Global Environment, Proceedings of the British Hydrological Society, Newcastle University, U. K., British Hydrological Society, Newcastle, United Kingdom, 21–23 July 2010.

Fewtrell, T. J., A. Duncan, C. C. Sampson, J. C. Neal, and P. D. Bates (2011), Benchmarking urban flood models of varying complexity and scale using high resolution terrestrial LiDAR data, *Phys. Chem. Earth*, *36*(7–8), 281–291, doi:10.1016/j.pce.2010.12.011.

Garcia, J. J. G. (2008), Sediment transport and morphodynamics, in *Sedimentation Engineering*, edited by J. J. G. Garcia, pp. 21–163, Am. Soc. of Civ. Eng., Reston, Va.

Guerrero, M., and A. Lamberti (2011), Flow field and morphology mapping using ADCP and multibeam techniques: Survey in the Po River, *J. Hydraul. Eng. ASCE*, *137*(12), 1576–1587, doi:10.1061/(asce)hy.1943–7900.0000464.

Guerrero, M., V. Di Federico, and A. Lamberti (2013), Calibration of a 2-D morphodynamic model using water–sediment flux maps derived from an ADCP recording, *J. Hydroinform.*, doi:10.2166/hydro.2012.126, in press.

Heritage, G. L., and D. J. Milan (2009), Terrestrial laser scanning of grain roughness in a gravel-bed river, *Geomorphology*, *113*(1–2), 4–11, doi:10.1016/j.geomorph.2009.03.021.

Heritage, G. L., D. J. Milan, A. R. G. Large, and I. C. Fuller (2009), Influence of survey strategy and interpolation model on DEM quality, *Geomorphology*, *112*(3–4), 334–344, doi:10.1016/j.geomorph.2009.06.024.

Hicks, D. M. (2012), Remotely sensed topographic change in gravel riverbeds with flowing channels, in *Gravel-Bed Rivers*, edited by M. Church, P. A. Biron, and A. G. Roy, pp. 303–314, John Wiley, Chichester, U. K., doi:10.1002/9781119952497.ch23.

Hicks, D. M., M. J. Duncan, J. M. Walsh, R. M. Westaway, and S. N. Lane (2001), New views of the morphodynamics of large braided rivers from high-resolution topographic surveys and time-lapse video, in *The Structure, Function and Mangement Implications of Fluvial Sedimentary Systems*, edited by F. J. Dyer, M. C. Thoms, and J. M. Olley, pp. 273–380, Int. Assoc. for Hydrol. Sci., Wallingford, U. K.

Hicks, D. M., U. Shankar, M. J. Duncan, M. Rebuffé, and J. Aberle (2009), Use of remote-sensing with two-dimensional hydrodynamic models to assess impacts of hydro-operations on a large, braided, gravel-bed river: Waitaki River, New Zealand, in *Braided Rivers*, edited by G. H. Sambrook Smith, et al., pp. 311–326, Blackwell Oxford, U. K., doi:10.1002/9781444304374.ch15.

Hilldale, R. C., and D. Raff (2008), Assessing the ability of airborne LiDAR to map river bathymetry, *Earth Surf. Processes Landforms.*, *33*(5), 773–783, doi:10.1002/esp.1575.

Hodge, R. A., D. A. Sear, and J. Leyland (2013), Spatial variations in surface sediment structure in riffle–pool sequences: A preliminary test of the differential sediment entrainment hypothesis (DSEH), *Earth Surf. Processes Landforms.*, *38*(5), 449–465, doi:10.1002/esp.3290.

Horritt, M. S. (2000), Calibration of a two-dimensional finite element flood flow model using satellite radar imagery, *Water Resour. Res.*, *36*(11), 3279–3291, doi:10.1029/2000wr900206.

Horritt, M. S. (2006), A methodology for the validation of uncertain flood inundation models, *J. Hydrol.*, *326*(1–4), 153–165, doi:10.1016/j.jhydrol.2005.10.027.

Hughes, M. L., P. F. McDowell, and W. A. Marcus (2006), Accuracy assessment of georectified aerial photographs: Implications for measuring lateral channel movement in a GIS, *Geomorphology*, *74*(1–4), 1–16, doi:10.1016/j.geomorph.2005.07.001.

Jamieson, E. C., C. D. Rennie, R. B. Jacobson, and R. D. Townsend (2011), 3-D flow and scour near a submerged wing dike: ADCP measurements on the Missouri River, *Water Resour. Res.*, *47*, W07544, doi:10.1029/2010wr010043.

Jowett, I. G., and M. J. Duncan (2012), Effectiveness of 1D and 2D hydraulic models for instream habitat analysis in a braided river, *Ecol. Eng.*, *48*, 92–100, doi:10.1016/j.ecoleng.2011.06.036.

Kalyanapu, A. J., S. Shankar, E. R. Pardyjak, D. R. Judi, and S. J. Burian (2011), Assessment of GPU computational enhancement to a 2D flood model, *Environ. Modell. Software*, *26*(8), 1009–1016, doi:10.1016/j.envsoft.2011.02.014.

Kleinhans, M. G., H. R. A. Jagers, E. Mosselman, and C. J. Sloff (2008), Bifurcation dynamics and avulsion duration in meandering rivers by one-dimensional and three-dimensional models, *Water Resour. Res.*, *44*, W08454, doi:10.1029/2007wr005912.

Lamb, R., M. Crossley, and S. Waller (2009), A fast two-dimensional floodplain inundation model, *Proc. Inst. Civ. Eng. Water Manage.*, *162*(6), 363–370, doi:10.1680/wama.2009.162.6.363.

Lane, S. N., J. H. Chandler, and K. S. Richards (1994), Developments in monitoring and modelling small-scale river bed topography, *Earth Surf. Processes Landforms.*, *19*(4), 349–368, doi:10.1002/esp.3290190406.

Lane, S. N., K. F. Bradbrook, K. S. Richards, P. A. Biron, and A. G. Roy (1999), The application of computational fluid dynamics to natural river channels: three-dimensional versus two-dimensional approaches, *Geomorphology*, *29*(1–2), 1–20, doi:10.1016/s0169–555x(99)00003-3.

Lane, S. N., R. M. Westaway, and D. M. Hicks (2003), Estimation of erosion and deposition volumes in a large, gravel-bed, braided river using synoptic remote sensing, *Earth Surf. Processes Landforms.*, *28*(3), 249–271, doi:10.1002/esp.483.

Legleiter, C. J., P. C. Kyriakidis, R. R. McDonald, and J. M. Nelson (2011), Effects of uncertain topographic input data on two-dimensional flow modeling in a gravel-bed river, *Water Resour. Res.*, *47*, W03518, doi:10.1029/2010wr009618.

Lesser, G. R., J. A. Roelvink, J. A. T. M. van Kester, and G. S. Stelling (2004), Development and validation of a three-dimensional morphological model, *Coast. Eng.*, *51*(8–9), 883–915, doi:10.1016/j.coastaleng.2004.07.014.

Marcus, W. A. (2012), Remote sensing of the hydraulic environment in gravel-bed rivers, in *Gravel-Bed Rivers*, edited by M. Church, P. A. Biron, and A. G. Roy, pp. 259–285, John Wiley, Chichester, U. K., doi:10.1002/9781119952497.ch21.

Marcus, W. A., and M. A. Fonstad (2008), Optical remote mapping of rivers at sub-meter resolutions and watershed extents, *Earth Surf. Processes. Landforms.*, *33*(1), 4–24, doi:10.1002/esp.1637.

McKean, J. A., D. J. Isaak, and C. W. Wright (2008), Geomorphic controls on salmon nesting patterns described by a new, narrow-beam terrestrial-aquatic lidar, *Front. Ecol. Environ.*, *6*(3), 125–130, doi:10.1890/070109.

McMillan, H., T. Krueger, and J. Freer (2012), Benchmarking observational uncertainties for hydrology: Rainfall, river discharge and water quality, *Hydrol. Processes.*, *26*(26), 4078–4111, doi:10.1002/hyp.9384.

Milan, D. J. (2009), Terrestrial laser scan-derived topographic and roughness data for hydraulic modelling of gravel-bed rivers, in *Laser Scanning for the Environmental Sciences*, edited by G. L. Heritage and A. R. G. Large, pp. 133–146, Wiley-Blackwell, Chichester, U. K., doi:10.1002/9781444311952.ch9.

Milan, D. J., and G. L. Heritage (2012), LiDAR and ADCP Use in Gravel-Bed Rivers: Advances since GBR6, in *Gravel-Bed Rivers*, edited by M. Church, P. A. Biron, and A. G. Roy, pp. 286–302, John Wiley, Chichester, U. K., doi:10.1002/9781119952497.ch22.

Milan, D. J., G. L. Heritage, and D. Hetherington (2007), Application of a 3D laser scanner in the assessment of erosion and deposition volumes and channel change in a proglacial river, *Earth Surf. Processes Landforms.*, *32*(11), 1657–1674, doi:10.1002/esp.1592.

Milan, D. J., G. L. Heritage, A. R. G. Large, and I. C. Fuller (2011), Filtering spatial error from DEMs: Implications for morphological change estimation, *Geomorphology*, *125*, 160–171, doi:10.1016/j.geomorph.2010.09.012.

Millar, R. G. (1999), Grain and form resistance in gravel-bed rivers, *J. Hydraul. Res.*, *37*(3), 303–312, doi:10.1080/00221686.1999.9628249.

Morlock, S. E. (1995), Evaluation of acoustic doppler current profiler measurements of river discharge, *U.S. Geological Survey Water Resources Investigation Report 95-4218*, 41 pp., U.S. Geol. Surv., Indianapolis, Ind.

Murray, A. B. (2007), Reducing model complexity for explanation and prediction, *Geomorphology*, *90*(3–4), 178–191.

Murray, A. B., and C. Paola (1997), Properties of a cellular braided-stream model, *Earth Surf. Processes. Landforms.*, *22*(11), 1001–1025.

Muste, M., K. Yu, and M. Spasojevic (2004), Practical aspects of ADCP data use for quantification of mean river flow characteristics; Part 1: moving-vessel measurements, *Flow Meas. Instrum.*, *15*(1), 1–16, doi:10.1016/j.flowmeasinst.2003.09.001.

Muste, M., D. Kim, and V. Merwade (2012), Modern digital instruments and techniques for hydrodynamic and morphologic characterization of river channels, in *Gravel-Bed Rivers*, edited by M. Church, P. A. Biron, and A. G. Roy, pp. 315–341, John Wiley, Chichester, U. K., doi:10.1002/9781119952497.ch24.

Neal, J. C., T. J. Fewtrell, P. D. Bates, and N. G. Wright (2010), A comparison of three parallelisation methods for 2D flood inundation models, *Environ. Modell. Software*, *25*(4), 398–411, doi:10.1016/j.envsoft.2009.11.007.

Nicholas, A. P., and T. A. Quine (2007), Crossing the divide: Representation of channels and processes in reduced-complexity river models at reach and landscape scales, *Geomorphology*, *90*(3–4), 318–339, doi:10.1016/j.geomorph.2006.10.026.

Nicholas, A. P., et al. (2012), Modelling hydrodynamics in the Rio Paraná, Argentina: An evaluation and inter-comparison of reduced-complexity and physics based models applied to a large sand-bed river, *Geomorphology*, *169–170*, 192–211, doi:10.1016/j.geomorph.2012.05.014.

Otago Regional Council (2008), Channel morphology and sedimentaton in the Rees River, *Rep.*, 27 pp., Otago Reg. Counc., Dunedin, New Zealand.

Papanicolaou, A. N., M. Elhakeem, and B. Wardman (2011a), Calibration and verification of a 2D hydrodynamic model for simulating flow around emergent bendway weir structures, *J. Hydraul. Eng. ASCE*, *137*(1), 75–89, doi:10.1061/(asce)hy.1943–7900.0000280.

Papanicolaou, A. N., M. Elhakeem, D. Dermisis, and N. Young (2011b), Evaluation of the Missouri River shallow water habitat using a 2D-hydrodynamic model, *River Res. Appl.*, *27*(2), doi:10.1002/rra.1344.

Parker, G. T., R. L. Droste, and C. D. Rennie (2009), An objective test of stochastic behavior in riverine water quality models, *Water Sci. Technol.*, *59*(1), 159–165, doi:10.2166/wst.2009.765.

Parsons, D. R., J. L. Best, S. N. Lane, R. J. Hardy, R. Kostaschuk, D. Shugar, and O. Orfeo (2006), Morphology, flow and sediment transport over a natural 3D dune field: Rio Parana, Argentina, in *River Flow 2006, vols. 1 and 2*, edited by R. M. L. Ferreira, et al., pp. 997–1004, Taylor and Francis, London.

Pasternack, G. B., C. L. Wang, and J. E. Merz (2004), Application of a 2D hydrodynamic model to design of reach-scale spawning gravel replenishment on the Mokelumne River, California, *River Res. Appl.*, *20*(2), 205–225, doi:10.1002/rra.748.

Pasternack, G. B., A. T. Gilbert, J. M. Wheaton, and E. M. Buckland (2006), Error propagation for velocity and shear stress prediction using 2D models for environmental management, *J. Hydrol.*, *328*(1–2), 227–241, doi:10.1016/j.jhydrol.2005.12.003.

Rao, P. (2005), A parallel RMA2 model for simulating large-scale free surface flows, *Environ. Modell. Software*, *20*(1), 47–53, doi:10.1016/j.envsoft.2003.12.008.

Refsgaard, J. C., and H. J. Henriksen (2004), Modelling guidelines—Terminology and guiding principles, *Adv. Water Resour.*, *27*(1), 71–82, doi:10.1016/j.advwatres.2003.08.006.

Rennie, C. D., and R. G. Millar (2004), Measurement of the spatial distribution of fluvial bedload transport velocity in both sand and gravel, *Earth Surf. Processes Landforms.*, *29*(10), 1173–1193, doi:10.1002/esp.1074.

Rennie, C. D., and M. Church (2010), Mapping spatial distributions and uncertainty of water and sediment flux in a large gravel bed river reach using an acoustic Doppler current profiler, *J. Geophys. Res.*, *115*, F03035, doi:10.1029/2009JF001556.

Rennie, C. D., R. D. Williams, J. Brasington, D. Vericat, and D. M. Hicks (2012), Within-event spatially distributed bedload: linking fluvial sediment transport to morphological change, paper presented at Hydraulic Measurement and Experimental Methods Conference, Snowbird, Utah, 12–15 August 2012, American Society of Civil Engineers.

Richardson, W. R., and C. R. Thorne (2001), Multiple thread flow and channel bifurcation in a braided river: Brahmaputra-Jamuna River, Bangladesh, *Geomorphology*, *38*(3–4), 185–196, doi:10.1016/s0169–555x(00)00080-5.

Riley, J. D., and B. L. Rhoads (2012), Flow structure and channel morphology at a natural confluent meander bend, *Geomorphology*, *163–164*, 84–98, doi:10.1016/j.geomorph.2011.06.011.

Rinaldi, M., B. Mengoni, L. Luppi, S. E. Darby, and E. Mosselman (2008), Numerical simulation of hydrodynamics and bank erosion in a river bend, *Water Resour. Res.*, *44*(9), W09428, doi:10.1029/2008wr007008.

Ruther, N., J. Jacobsen, N. R. B. Olsen, and G. Vatne (2010), Prediction of the three-dimensional flow field and bed shear stresses in a regulated

river in mid-Norway, *Hydrol. Res.*, *41*(2), 145–152, doi:10.2166/nh.2010.064.

Rychkov, I., J. Brasington, and D. Vericat (2012), Computational and methodological aspects of terrestrial surface analysis based on point clouds, *Comput. Geosci.*, *42*, 64–70, doi:10.1016/j.cageo.2012.02.011.

Rye, C. J., I. C. Willis, N. S. Arnold, and J. Kohler (2012), On the need for automated multiobjective optimization and uncertainty estimation of glacier mass balance models, *J. Geophys. Res.*, *117*, F02005, doi:10.1029/2011JF002184.

Sampson, C. C., T. J. Fewtrell, A. Duncan, K. Shaad, M. S. Horritt, and P. D. Bates (2012), Use of terrestrial laser scanning data to drive decimetric resolution urban inundation models, *Adv. Water Resour.*, *41*, 1–17, doi:10.1016/j.advwatres.2012.02.010.

Simpson, M. R., and R. N. Oltmann (1993), Discharge measurement system using an acoustic Doppler current profiler with applications to large rivers and estuaries, *U.S. Geological Survey Water-Supply Paper 2395*, 32 pp., U.S. Geological Surv., Denver, Colo.

Smith, L. C., B. L. Isacks, A. L. Bloom, and A. B. Murray (1996), Estimation of discharge from three braided rivers using synthetic aperture radar satellite imagery: Potential application to ungaged basins, *Water Resour. Res.*, *32*(7), 2021–2034, doi:10.1029/96wr00752.

Spear, R. C., T. M. Grieb, and N. Shang (1994), Parameter uncertainty and interaction in complex environmental models, *Water Resour. Res.*, *30*(11), 3159–3169, doi:10.1029/94wr01732.

Stelling, G. S., and J. J. Leendertse (1992), Approximation of convective processes by cyclic AOI methods, in *Estuarine and Coastal Modeling*, edited by M. L. Spaulding, K. Bedford, and A. Blumberg, pp. 771–782, ASCE, Tampa, Fla.

Stewart, G., R. Anderson, and E. Wohl (2005), Two-dimensional modelling of habitat suitability as a function of discharge on two Colorado rivers, *River Res. Appl.*, *21*(10), 1061–1074, doi:10.1002/rra.868.

Szupiany, R. N., M. L. Amsler, D. R. Parsons, and J. L. Best (2009), Morphology, flow structure, and suspended bed sediment transport at two large braid-bar confluences, *Water Resour. Res.*, *45*, W05415, doi:10.1029/2008wr007428.

Thomas, R., and A. P. Nicholas (2002), Simulation of braided river flow using a new cellular routing scheme, *Geomorphology*, *43*(3–4), 179–195.

Thomas, R., A. P. Nicholas, and T. A. Quine (2007), Cellular modelling as a tool for interpreting historic braided river evolution, *Geomorphology*, *90*(3–4), 302–317, doi:10.1016/j.geomorph.2006.10.025.

Turnbull, I. M. (2000), *Geology of the Wakatipu Area*, 72 pp., Inst. of Geol. & Nucl. Sciences Limited, Lower Hutt, New Zealand.

Van De Wiel, M. J., T. J. Coulthard, M. G. Macklin, and J. Lewin (2007), Embedding reach-scale fluvial dynamics within the CAESAR cellular automaton landscape evolution model, *Geomorphology*, *90*(3–4), 283–301.

Van De Wiel, M. J., T. J. Coulthard, M. G. Macklin, and J. Lewin (2011), Modelling the response of river systems to environmental change: Progress, problems and prospects for palaeo-environmental reconstructions, *Earth Sci. Rev.*, *104*(1–3), 167–185.

van der Wegen, M., and J. A. Roelvink (2008), Long-term morphodynamic evolution of a tidal embayment using a two-dimensional, process-based model, *J. Geophys. Res.*, *113*, C03016, doi:10.1029/2006JC003983.

van der Wegen, M., Z. B. Wang, H. H. G. Savenije, and J. A. Roelvink (2008), Long-term morphodynamic evolution and energy dissipation in a coastal plain, tidal embayment, *J. Geophys. Res.*, *113*, F03001, doi:10.1029/2007JF000898.

van der Wegen, M., B. E. Jaffe, and J. A. Roelvink (2011), Process-based, morphodynamic hindcast of decadal deposition patterns in San Pablo Bay, California, *J. Geophys. Res.*, *116*, F02008, doi:10.1029/2009JF001614.

Westaway, R. M., S. N. Lane, and D. M. Hicks (2003), Remote survey of large-scale braided, gravel-bed rivers using digital photogrammetry and image analysis, *Int. J. Remote Sens.*, *24*(4), 795–815, doi:10.1080/01431160110113070.

Wheaton, J. M., J. Brasington, S. E. Darby, and D. A. Sear (2010), Accounting for uncertainty in DEMs from repeat topographic surveys: improved sediment budgets, *Earth Surf. Processes Landforms.*, *35*(2), 136–156, doi:10.1002/esp.1886.

Wild, M., T. Cochrane, T. Davies, D. M. Hicks, D. Painter, and G. Palmer (2008), Recent sedimentation rates for the Rees-Dart braided river delta, paper presented at Sediment Dynamics in Changing Environments, Christchurch, New Zealand, The International Association of Hydrological Sciences, 1-5 December 2008.

Williams, R. D., J. Brasington, D. Vericat, and D. M. Hicks (2013), Hyperscale terrain modelling of braided rivers: fusing mobile terrestrial laser scanning and optical bathymetric mapping, *Earth Surf. Processes Landforms.*, doi:10.1002/esp.3437.

Williams, R. D., J. Brasington, D. Vericat, D. M. Hicks, F. Labrosse, and M. Neal (2011), Monitoring braided river change using terrestrial laser scanning and optical bathymetric mapping, in *Geomorphological Mapping: Methods and Applications*, edited by M. Smith, P. Paron, and J. Griffiths, pp. 507–532, Elsevier, Amsterdam, doi:10.1016/B978-0-444–53446-0.00020-3.

Wolman, M. G. (1954), A method of sampling coarse bed material, *Trans. AGU*, *35*, 951–956.